Effect of Asymmetric Topography on Rupture Propagation along Fault Stepovers

Roby Douilly[1]

[1]University of California, Riverside

February 9, 2023

Abstract

Complex fault systems are often located in regions with asymmetric topography on one side of a fault, and these systems are very common in Southern California. Along these fault systems, geometrical complexities such as stepovers can impact fault rupture. Previous rupture dynamic studies have investigated the effect of stepover widths on throughgoing rupture, but these studies didn't examine the influence of topography on the rupture behavior. To investigate the effect of asymmetric topography on rupture dynamics at stepovers, I consider three cases: 1) a flat topography, 2) a positive (mountain) and 3) a negative (basin) topography on only one side of the fault system outside of the stepover. In each case, I use the 3D finite element method to compute the rupture dynamics of these fault systems. The results show a significant time dependent variation of the normal stress for the topography cases as opposed to the flat surface case, which can have an important impact on rupture propagation at the stepover. For a positive topography on the right of the rupture propagation, there is a clamping effect behind the rupture front that prevents the rupture to jump a wider extensional stepover. The opposite is observed for a negative topography or for a positive topography on the left side of the rupture propagation, where the rupture can jump over a wider compressional stepover. These results suggest that topography should be considered in dynamic studies with geometric complexities such as stepovers, and perhaps bends and branched fault systems.

Effect of Asymmetric Topography on Rupture Propagation along Fault Stepovers

Roby Douilly
University of California, Riverside

Corresponding author: Roby Douilly (roby.douilly@ucr.edu)

Key points:

- Asymmetric topography can affect rupture propagation across fault stepovers
- Topography can cause a clamping or unclamping effect that can prevent or facilitate a rupture to jump a wider extensional stepover
- With topography, changing the hypocenter location can have a significant impact on throughgoing rupture across fault stepovers.

Abstract:

Complex fault systems are often located in regions with asymmetric topography on one side of a fault, and these systems are very common in Southern California. Along these fault systems, geometrical complexities such as stepovers can impact fault rupture. Previous rupture dynamic studies have investigated the effect of stepover widths on throughgoing rupture, but these studies didn't examine the influence of topography on the rupture behavior. To investigate the effect of asymmetric topography on rupture dynamics at stepovers, I consider three cases: 1) a flat topography, 2) a positive (mountain) and 3) a negative (basin) topography on only one side of the fault system outside of the stepover. In each case, I use the 3D finite element method to compute the rupture dynamics of these fault systems. The results show a significant time dependent variation of the normal stress for the topography cases as opposed to the flat surface case, which can have an important impact on rupture propagation at the stepover. For a positive topography on the right of the rupture propagation, there is a clamping effect behind the rupture front that prevents the rupture to jump a wider extensional stepover. The opposite is observed for a negative topography or for a positive topography on the left side of the rupture propagation, where the rupture can jump over a wider compressional stepover. These results suggest that topography should be considered in dynamic studies with geometric complexities such as stepovers, and perhaps bends and branched fault systems.

Plain Language Summary:

Topography such as a mountain range or a basin can be found near faults across the world. This work investigates whether a surface topography can affect an earthquake to propagate across fault stepovers which are discontinuous faults with an offset of some distance with one another. I use three-dimensional dynamic models to generate a number of earthquake scenarios using different types of topography (mountain or basin). I find that the type of topography can sometimes prevent or facilitate an earthquake rupture to propagate across a fault stepover. While numerical experiment without topography has shown it is unlikely for an earthquake to propagate across a stepover width greater than 4 km, adding topography can cause the rupture to jump beyond 4 km. This result could be a potential explanation as to why some past earthquakes are able to jump a stepover width of 4 km or greater while others couldn't and it could have real hazard implications for future earthquakes on stepovers.

1. Introduction

Major earthquakes often involve multiple fault segments by propagating across geometric complexities such as fault stepover. One important example is the 1968 Borrego mountain earthquake (Wesnousky, 1988). During this event, the rupture was able to propagate across a 1.5 km restraining step but couldn't jump a releasing stepover of 7 km nor a restraining stepover of 2.5 km. Other more recent earthquakes such as the 1992 Landers earthquake (Wald & Heaton, 1994), the 1999 Izmit earthquake (Ozalaybey et al., 2002), and the 2019 Ridgecrest sequence (Ross et al., 2019) involved rupture propagating across fault stepovers, with the width of those jumped stepovers not exceeding 4 km. Understanding whether a rupture is likely to jump across a stepover during a single event is crucial, as it will affect the overall earthquake size. Wesnousky, (2006) analyzed surface traces of 22 historical strike-slip earthquakes and found that no events within that group were able to jump a width of 5 km or above. Furthermore, very few earthquakes were able to jump a stepover width of 3-4 km, and 40% of the events below that threshold also didn't propagate across. The Uniform California Earthquake Rupture Forecast 3 (UCERF3) seismic hazard analysis even incorporates a 5 km limit above which a single rupture cannot jump (Field et al., 2014). However, a few exceptional earthquakes have been observed where the rupture appeared to jump a step greater than 5 km. The 2010 El Mayor-Cucapah earthquake ruptured across a 120 km long multi-fault segments and the rupture appeared to propagate across a 10 km wide stepover with potentially intermediary sub-faults (Oskin et al., 2012). The 2016 Kaikoura New Zealand earthquake ruptured more than a dozen fault segments with apparent rupture jump stepovers greater than 15 km (Kaiser et al., 2017; Ulrich et al., 2019). Therefore, it is important to proper evaluate the factors that could limit or facilitate a rupture to jump across wide stepovers.

A number of numerical modeling studies have attempted to point out some key physical parameters (*i.e.* fault geometry, initial stress and frictional parameters) that could affect throughgoing rupture across stepovers. Fault geometry is clearly a major effect in rupture propagation. Harris et al., (1991) and Harris & Day, (1993) performed 2D dynamic models of a series of super-shear ruptures across strike-slip fault steps for various stepover widths (1-6 km). They found that the rupture could jump across both a restraining and releasing stepover, and argued that the rupture is unlikely to jump a releasing stepover wider than 5 km and restraining stepover wider than 2.5 km. The seismogenic depth of a fault is another controlling effect where rupture on a fault with large seismogenic depth can jump wider stepovers (Bai & Ampuero, 2017). Furthermore, the frictional properties could also affect rupture propagation. Ryan & Oglesby, (2014) argued that the likelihood for a rupture to jump large stepovers is dependent on the friction parameterization used where rate and state friction with strong rate-weakening can facilitate the rupture to jump over large stepovers (> 7km). Other studies have found that the choice of the slip-weakening distance can also affect throughgoing rupture across stepovers where increasing the slip-weakening distance can prevent a rupture from jumping across a stepover and vice-versa (Lozos et al., 2014). Moreover, Liu & Duan, (2016) argued that there is a linear relationship between the maximum jumpable stepover and the slip gradient where a larger stress drop will

facilitate the rupture to jump a wider stepover. Another key factor to consider is the heterogeneity in the state of stress particularly near the geometrical discontinuities. While homogeneous stress is usually assumed in previous dynamic rupture models, Duan & Oglesby, (2007) show that over multiple earthquake cycles, a heterogeneous fault stress field can develop near a fault branch due to the interactions of the different segments, and this could impact the ability of rupture to propagate across the stepover. Furthermore, significant stress variations are observed near stepovers due to long-term fault tectonics (Wang et al., 2017; Ye et al., 2015). Harris & Day, (1999) mentioned that heterogenous stress distribution can affect rupture where earthquakes occurring on faults close to failure, due to a prior rupture, may jump wider stepovers. More recently, Wang et al., (2020) use 2D dynamic rupture models to investigate the effect of heterogenous fault stress from long term simulation on fault stepovers. They argued that a rupture can jump up to 20 km across overlapping releasing stepovers and up to 7 km across restraining stepovers.

Some recent dynamic studies have started to incorporate surface topography in their modeling despite the increased level of complexity it poses (Ulrich et al., 2019; Wollherr et al., 2019). Adding topography involves technical challenges—it will not only make the volume more difficult to mesh, but it will require significantly more processing power and a longer computational time. Nevertheless, surface topography has been seen to cause noticeable fluctuations in rupture behavior for scenarios of earthquakes on a single fault segment. Zhang et al., (2016) modeled rupture dynamics on a fault with varying topographic surfaces and they argued that depending on the shape (hill or valley) and epicentral distance to the fault, topography can affect the sub-shear to super-shear transition. More recently, Kyriakopoulos et al., (2021) investigated the effect of asymmetric topography on a single fault and found that the position of the topography with respect to the rupture propagation can either cause a positive (clamping effect) or negative (unclamping effect) normal stress perturbation behind the rupture front and an opposite normal stress effect ahead of the rupture front. In addition, most major fault systems tend to be located in region with asymmetric topography. This type of asymmetric topography next to a fault system can be seen at several location around southern California. As an example, mountain ranges can be seen primarily between the fault segmentation that ruptured during the 2010 El Mayor-Cucapah earthquake (Oskin et al., 2012). Also, the left-lateral Garlock fault system, which is composed of two segments separated by an extensional stepover width of 3-4 km, has high mountain ranges on its northern side and almost a flat topography on the southern side. This stepover is particularly important because the recent 2019 Ridgecrest sequence triggered significant seismicity on the Garlock fault (Cochran et al., 2020; Shelly, 2020) and an important increase in shear stress was also observed on that segment near the segmentation (Ramos et al., 2020). Considering that the aforementioned stepover modeling studies assumed a flat topography and didn't explore whether surfaces with irregular topographies can also impact rupture propagation across fault segmentation, it is worth investigating whether topography can also affect rupture jump across fault stepovers.

Here I use 3-D dynamic rupture simulations to investigate if mountain ranges (positive topography) or valleys (negative topography) can facilitate or hinder a rupture from propagating across a vertical strike-slip fault stepover. I will vary the position and shape of the geometry with respect to the stepover to understand which details of the model have controlling effects on rupture behavior.

2. Model setup and computational parameters

The main objective of this study is to highlight the effects asymmetric topography can have on fault segmentation. I consider the stepover to be composed of two vertical planar fault segments (fault 1 and fault 2) of 30 km each with 15 km locking depth and with a 5 km overlap. I explore offsets or stepover widths that vary from 2 to 8 km. A synthetic topography with a Rayleigh distribution (Figure 1) is added on the northern portion of the stepover so that the fault system has no elevation (the fault system is on the free surface at 0 km) and the topography is distributed over a 30 km horizontal distance perpendicular to strike (Figure 1). For each geometry, I consider three different types of topography: 1) a no topography case which will serve as a comparison to other dynamic model studies (*e.g.*, Harris et al., 1991; Harris & Day, 1993), 2) a positive topography case (or mountain range) and 3) a negative topography case (or valley). For all geometries, we build a three-dimensional finite element mesh using the Cubit software version 2021.5, with the model space discretized with hexahedral elements of 200 m size within and around the volume hosting the faults, but becoming coarser (800 m) away from the fault system (see inset in Figure 1).

The meshes are then imported into the 3-D finite element code FaultMod (Barall, 2009), which has been validated through the Southern California Earthquake Data Center community rupture verification code (Harris et al., 2009; 2018). To implement the dynamic rupture models, I consider a uniform pre-stress conditions (Table 1) with strength parameter (S) of 0.5, which leads to super-shear rupture similar to the modeling studies of Harris & Day, (1993). The S value is the ratio between the strength excess (yield stress minus initial stress) and the dynamic stress drop (initial shear stress minus sliding stress) as defined by Das & Aki, (1977). I implement the stress conditions so that the faults have a left-lateral strike-slip motion consistent with the releasing stepover on the Garlock fault, but for completeness I also test scenarios for a restraining stepover (or a right-lateral strike-slip motion) on the faults. The friction law used in this study is the linear slip-weakening (Andrews, 1976; Ida, 1972) where I assume a slip-weakening distance, static friction and dynamic friction of 0.4 m, 0.75 and 0.3 respectively. However, since Lozos et al. (2014) inferred that decreasing the slip-weakening distance could facilitate the rupture to jump across a wider stepover (Lozos et al., 2014), I also test cases with slip-weakening distance of 0.3 m. Table 1 summarizes the values of all the computational parameters for the rupture simulations conducted in this study.

3. Results

For each scenario, I nucleate the rupture at the same location on fault 1 (green fault in Figure 1) by creating a circular region in which the shear stress is 10% greater than the failure stress so that the nucleation zone ruptures instantaneously and analyze whether topography affects the rupture behavior on both fault (fault 1 and fault 2) of the stepover system. In the following, the nucleated segment will be referred to as source fault and the other segment of the stepover as receiver fault. Figure 2 shows the evolution of slip for the three geometries (flat, positive, and negative topographies) with a releasing stepover width of 4 km and for a slip-weakening distance of 0.4 m. On the source fault (fault 1 in this case), the type of topography does not change the rupture speed, but it does affect the total slip. With a topography on the right of the rupture propagation for a left-lateral strike-slip fault (releasing stepover), a positive topography causes less slip to develop on the source fault as opposed to the flat case. On the other hand, more slip is observed for the negative topography compared to the flat case. Furthermore, adding topography affects the ability for a rupture to jump across the stepover. For the flat topography case and for a slip-weakening distance of 0.4 m, the rupture jumps across the stepover and triggers small slip on the receiver fault (purple ellipse in Figure 2), but the rupture rapidly dies out. However, a positive topography prevents the rupture from jumping across, while a negative topography facilitates the rupture to jump, and the rupture breaks the receiver fault in its entirety.

Kyriakopoulos et al. (2021) investigated the impact of asymmetric topography along a single vertical fault, and they showed that with topography on the right of propagating rupture for a right lateral strike-slip fault, there is clamping (increase of normal stress) ahead of the rupture front and unclamping (decrease of normal stress) behind the rupture front; the effect reverses when the mountains are on the opposite side of the fault. I also observe these normal stress perturbations, and they affect rupture propagation across a fault stepover. Figure 3 shows the normal stress change at sequential time steps for the three topographic cases (flat, positive, and negative topography) on the releasing stepover. For the flat topography, there is no significant normal stress perturbation. For a positive topography on the right of the rupture propagation for left-lateral strike-slip fault, there is a decrease in normal stress (unclamping) ahead of the rupture front and an increase in normal (clamping) stress behind the rupture front, consistent with Kyriakopoulos et al. (2021). The opposite is observed for the negative topography, where there is an unclamping behind the rupture front a clamping ahead of the rupture front. These perturbations cause fluctuations in normal stress on the receiver fault. Figure 4 shows the time evolution of slip, shear stress and normal stress on points on fault 1 and fault 2 as located in Figure 3. The topography induced normal stress perturbation behind the rupture front on the source fault is much larger compared to the one ahead of the rupture, and is the leading factor to affect rupture propagation. For the negative topography, the unclamping effect behind the rupture front on fault 1 induces a decrease in normal stress on fault 2 on top of the overall normal stress decrease caused by the extensional stepover. This additional decrease causes the shear stress to overcome the failure stress and thus triggers slip on fault 2. On the other hand, the clamping effect behind the rupture front

for the positive topography case on the right side of the rupture propagation for a releasing stepover causes a normal stress increase on fault 2 that pushes the fault further away from failure. Therefore, the addition of topography can significantly alter the outcome of a rupture propagation across a stepover.

Another important observation is that the addition of topography affects the peak slip near the free surface. Amplified slip near the free surface causes the rupture to trigger the receiver fault near the surface instead of at depth as it is for the flat case. This is most likely due to the fact that the topographically-induced normal stress perturbations are higher near the surface and decrease with depth, also consistent with Kyriakopoulos et al. (2021) (Figure 3). To further explore this issue, I consider scenarios using the same frictional conditions as in Figure 2 (slip-weakening distance of 0.4 m) but in addition, I linearly taper the shear and normal stresses in the upper 3 km. Figure 5 and supplemental video 1 show the final slip for the negative topography case for releasing stepover widths of 4 km and 5 km with non-tapered (upper panels) and tapered (lower panels) initial stress conditions. Similar to the fully homogeneous stress cases, ruptures are still being triggered close to the free surface and not at depth as it is for the flat topography case. It is worth noting that increasing the gap not only causes a decrease of the maximum slip on the receiver fault but also leads to a delay triggering of the receiver fault. However, tapering the stresses in the upper few kilometers does limit throughgoing rupture across wider step over since less slip develops on both faults. Despite the decrease in the maximum slip, the rupture was able to jump across the releasing stepover for a 4 km gap but couldn't propagate a stepover width of 5 km. Considering Lozos et al., (2014) pointed out for the flat topography case that decreasing the slip-weakening distance does facilitate the rupture to jump a wider stepover, I also explore scenarios for a reduced slip-weakening distance value. I re-run the models described above by decreasing the slip-weakening distance from 0.4 m to 0.3 m for all three types of topography for stepover width of 4 km. For the flat case topography, decreasing the slip-weakening does allow the rupture to easily propagate across the stepover (Figure 6; supplemental video 2). However, a positive topography north of the fault system still prevents a throughgoing rupture across this releasing stepover. Topography also affects the triggering time on the receiver fault (fault 2). As shown in Figure 6, a negative topography north of the releasing stepover causes an early triggering of the receiver fault compared to the flat topography case.

4. Discussion

4.1. Impact of stepover gap and type of topography on throughgoing rupture

The rupture simulations described above show that topography (positive or negative) can affect rupture jumping across a stepover width of 4 or 5 km. But while there have been few real-world observations of such jumps, there have been some past earthquakes where the rupture appeared to jump a step greater than 4 km (Oskin et al., 2012; Ulrich et al., 2019). Previous dynamic modeling studies have shown that parameters such as slip-weakening distance (Lozos et al., 2014), friction law (Ryan et al., 2014), stress heterogeneity (Wang et al., 2020), seismogenic depth (Bai and

Ampuero, 2017), pore pressure (Liu and Duan, 2014) and slip gradient (Liu & Duan, 2016; Oglesby, 2008) can enable rupture to jump wider stepovers. To further investigate the impact of topography on stepover width, I generate more scenarios with stepover widths that vary from 2 to 8 km for a slip-weakening distance of 0.4 m. A detailed summary of the rupture behavior for various stepover widths is shown in Figure 7. In this analysis, a triggering time is considered when the slip rate on the receiver fault reaches a value of 0.1 m/s. For the flat case, the result is consistent with Harris and Day, (1999) which argued that a rupture rarely jumps across wide stepovers. Overall, a negative topography allows the rupture to jump across a wider stepover (max 6 km for an extensional stepover – see supplemental video 3) and it also causes an early triggering on the receiver fault as opposed to the flat and positive topography.

Adding a positive topography or mountain ranges can significantly alter rupture behavior across a fault stepover. In all the previous simulations, we assumed a fixed topography base width of 30 km that is distributed away from fault 1. Considering mountain ranges can be wide or narrow near a fault system, it is worth understanding whether a decrease of the base width would have any effect. Therefore, I consider 2 more scenarios with a base width of 20 km and 10 km respectively (see Figure 1). Figure 8 shows the final slip for the flat case (panel A), the positive topography with 30 km base width (panel B, same as in Figure 2), the positive topography with 20 km base width (panel C) and the positive topography with 10 km base width (panel D). While a wide base width prevents the rupture from jumping across the stepover for a rupture initiated on fault 1, decreasing the base width facilitates a throughgoing rupture (Supplemental video 4 and panel D in Figure 8). Figure 9 shows the normal stress changes at two different timestep for the cases shown in Figure 8. As shown above, a positive topography on the right side of the rupture propagation cause a clamping effect behind the rupture front for a releasing stepover that prevents the rupture from jumping across the stepover. However, for a positive topography distributed over a narrower distance (base width in the order of 10-20 km), following the clamping phase, there is a delayed unclamping effect (purple ellipse in Figure 9). For the base topography width of 20 km, the delayed unclamping phase is enough to facilitate the triggering of the receiver fault (fault 2) but the rupture rapidly dies out. Moreover, for the base width of 10 km, the trailing decrease in normal stress facilitates the rupture to jump across the extensional stepover and ruptures fault 2 entirely. Kyriakopoulos et al., (2021) argued that these dynamic normal stress perturbations are analogous to the normal stress change thrust faults cause inside and outside the slipping region. Therefore, I could argue that while a positive slope for the mountain side closest to the fault system does induce a clamping effect when the positive topography is on the right side of the rupture propagation, the negative side of the mountain side, which is further away from the system, would cause an opposite effect (unclamping) as shown in the Figure 9. Therefore, for a wider topography base width, I hypothesize that the delayed dynamic phases (Figure 9) are most likely attenuated with distance, which would explain why those delayed phases are not seen for the 30 km base width. This would suggest that these dynamic normal stress changes are dependent on the distance of the topography

to the fault system and thus topography that is far away from a fault system is unlikely to induce any normal stress perturbation.

4.2. Rupture behavior impacted by slip motion and hypocenter location

Ruptures on extensional stepovers are more prone to throughgoing rupture and are more likely to jump wider gap compared to ruptures on compressional stepovers (Harris et al., 1991; Harris and Day, 1993; Wang et al., 2020). Considering for an extensional stepovers, a positive topography on the right side of the rupture propagation causes a clamping effect behind the rupture front that can prevent throughgoing rupture, a compressional stepover (reversal of the slip direction or changing the system from a left-lateral to a right-lateral strike-slip) with those same conditions will cause the opposite effect (unclamping) behind the rupture front and thus could potentially facilitate the rupture to jump across. Therefore, I generate more rupture simulations across a restraining stepover for a range of stepover widths (2nd column of Figure 7). For a slip-weakening distance of 0.4 m, a rupture on a compressional stepover couldn't jump a stepover width of 4 km for both the flat and positive topography. However, when I decrease the slip-weakening distance from 0.4 m to 0.3 m, a positive topography on the right side of the rupture propagation still prevents a rupture from propagating across a releasing stepover width of 4 km, while numerical experiment shows that the rupture could easily jump across this stepover for the positive topography on a restraining stepover (Supplemental video 2). This is most likely due to the fact that positive topography on the right side of a restraining stepover (reversal of the slip direction) causes an unclamping behind the rupture as opposed to a clamping effect for the releasing stepover. However, unlike our previous scenarios where the triggering takes place within the overlapping region, for the restraining stepover, the rupture not only triggers at a distance outside the overlapping region but also an early triggering is observed on the receiver fault compare to the releasing stepover case (Figure 7). While the throughgoing rupture across the restraining stepover occurred because of the positive topography, the location of the triggering on the receiver fault is not associated with the topography. Harris et al., (1991) and Harris and Day, (1993) reported that releasing steps trigger later than restraining step and the initial point of rupture on the receiver fault is located away from the overlapping region. Furthermore, consistently with Harris et al., 1991 and Harris and Day, 1993, the bigger the width of the restraining stepover, the greater the triggering distance.

For all the scenarios above, I assume the same hypocenter location on fault 1. For the flat topography case, since the segments are planar and the initial stress conditions are homogeneous, the rupture pattern would be the same whether the hypocenter is on fault 1 or fault 2. However, considering that the dynamic normal stress fluctuations induced by the addition of topography vary with respect to the direction of the rupture propagation, moving the hypocenter to the other fault for the topography cases should lead to very different rupture behaviors. Therefore, I modified the geometry shown in Figure 1 (see Figures 10A and 10D) so that the positive topography follows the fault system across the stepover, staying close to fault 2 (instead of at a distance as it is in

Figure 1), considering that the induced normal stress perturbations attenuate if the topography is distant from the fault system. Figure 10E shows the final slip for a rupture initiated on fault 2 with a releasing stepover width of 4 km and for a slip-weakening distance of 0.4 m. While a rupture nucleated on fault 1 couldn't propagate all the way through the stepover for the positive topography case (Figure 10B and supplemental video 5), a rupture nucleated on fault 2 propagates very easily across the stepover. This is because for a rupture initiated on fault 2, the positive topography is on the left side of the rupture propagation and thus the normal stress perturbations are reversed compared to the cases in which the positive topography is on the right side. In particular, this shift causes a decrease in normal stress behind the rupture front that facilitates the rupture to jump across to fault 1 (Figure 10F). With the addition of topography alone, the location of the hypocenter either hinders or facilitates a rupture to propagate across a stepover. Therefore, this observation could be a potential explanation as to why some past earthquakes are able to jump a stepover width of 4 km or greater while others couldn't. Furthermore, this result has real hazard implications for future earthquakes on stepovers such as the one along the Garlock fault system. This would suggest that it is more likely for a rupture initiated on the Garlock fault close to the Ridgecrest region to stop at the stepover than a rupture initiated on the Garlock fault close to the San Andreas junction.

5. Conclusion

In this study, I used 3D dynamic rupture simulation to investigate the effect of topography on rupture propagation across releasing and restraining stepover. I consider three cases (flat topography, positive topography and negative topography) and assume a homogeneous stress conditions with a S value of 0.5. I find that asymmetric topography has a significant impact in influencing throughgoing rupture across fault stepovers. For a positive topography on the right of the rupture propagation for a left-lateral fault, there is clamping effect behind the rupture front that prevents the rupture to jump a wider extensional stepover. On the other hand, for a negative topography, an unclamping effect is observed behind the rupture front that facilitate the rupture to jump across a wider extensional stepover. While positive topography can hinder a rupture from propagating across a releasing stepover, rupture can easily jump across for the positive topography on a restraining stepover for a slip-weakening distance of 0.3 m and a stepover width of 4 km.

We can also observe that the topography doesn't change the rupture speed on the source fault, but it does affect the triggering time on the receiver fault. A negative topography on the north of the releasing stepover causes an early triggering of the receiver fault relative to a flat model. The topography base width can also affect through-going rupture. Although positive topography (on the right side of the rupture propagation) distributed over a wider distance can prevent a rupture from jumping across a releasing stepover, decreasing the base width of the topography (i.e., a narrower mountain range) can facilitate the rupture jumping across the stepover. Furthermore, changing the hypocenter location to fault 2 for the positive topography case will cause an unclamping effect behind the rupture front that can facilitate the rupture to jump across the stepover.

These results have strong implications for real case such as the 4 km gap releasing stepover on the eastern Garlock fault system, which has a positive topography north of the system that is distributed over a larger distance. My results would imply that it is less likely for a rupture initiated on the Garlock segment close to the Ridgecrest region to jump across this stepover due to the topography but more likely for a throughgoing rupture to occur if the rupture is initiated close to the San Andreas fault. However, I have to point out that the current models don't take into account factors such as depth dependent stresses (Aochi & Tsuda, 2023), stress heterogeneity (Douilly et al., 2020; Duan & Oglesby, 2007; Wang et al., 2020) and off-fault plasticity (Gabriel et al., 2013) that could also affect the likelihood of throughgoing rupture. This is particularly important considering that the 2019 Ridgecrest caused an increase in stress on the Garlock fault segment near the segmentation (Ramos et al., 2020). In addition, Toda & Stein, (2020) showed an increase in Coulomb stress change on the section of the Garlock fault closer to the San Andreas fault. Therefore, future studies that include heterogeneous shear stress, depth dependent normal stress and off-fault plasticity should be considered to further investigate the impact of topography on fault stepovers. Moreover, considering how topography can either hinder or facilitate rupture, future studies should also investigate whether topography has similar effect on other geometrical discontinuities such as branch fault system with variable dip angles.

References

Andrews, D. (1976). Rupture propagation with finite stress in antiplane strain. *Journal of Geophysical Research*, *81*(20), 3575–3582.

Aochi, H., & Tsuda, K. (2023). Dynamic rupture simulations based on depth-dependent stress accumulation. *Geophysical Journal International*, *233*(1), 182–194.

Bai, K., & Ampuero, J.-P. (2017). Effect of seismogenic depth and background stress on physical limits of earthquake rupture across fault step overs. *Journal of Geophysical Research: Solid Earth*, *122*(12), 10–280.

Barall, M. (2009). A grid-doubling finite-element technique for calculating dynamic three-dimensional spontaneous rupture on an earthquake fault. *Geophysical Journal International*, *178*(2), 845–859.

Cochran, E. S., Wolin, E., McNamara, D. E., Yong, A., Wilson, D., Alvarez, M., van der Elst, N., McClain, A., & Steidl, J. (2020). The US Geological Survey's rapid seismic array deployment for the 2019 Ridgecrest earthquake sequence. *Seismological Research Letters*.

Das, S., & Aki, K. (1977). A numerical study of two-dimensional spontaneous rupture propagation. *Geophysical Journal International*, *50*(3), 643–668.

Douilly, R., Oglesby, D. D., Cooke, M. L., & Hatch, J. L. (2020). Dynamic models of earthquake rupture along branch faults of the eastern San Gorgonio Pass region in California using complex fault structure. *Geosphere*, *16*(2), 474–489.

405 Duan, B., & Oglesby, D. D. (2007). Nonuniform prestress from prior earthquakes and the effect
406 on dynamics of branched fault systems. *Journal of Geophysical Research: Solid Earth*,
407 *112*(B5).
408 Field, E. H., Arrowsmith, R. J., Biasi, G. P., Bird, P., Dawson, T. E., Felzer, K. R., Jackson, D.
409 D., Johnson, K. M., Jordan, T. H., Madden, C., & others. (2014). Uniform California
410 earthquake rupture forecast, version 3 (UCERF3)—The time-independent model. *Bulletin*
411 *of the Seismological Society of America*, *104*(3), 1122–1180.
412 Gabriel, A.-A., Ampuero, J.-P., Dalguer, L., & Mai, P. M. (2013). Source properties of dynamic
413 rupture pulses with off-fault plasticity. *Journal of Geophysical Research: Solid Earth*,
414 *118*(8), 4117–4126.
415 Harris, R. A., Archuleta, R. J., & Day, S. M. (1991). Fault steps and the dynamic rupture
416 process: 2-D numerical simulations of a spontaneously propagating shear fracture.
417 *Geophysical Research Letters*, *18*(5), 893–896.
418 Harris, R. A., & Day, S. M. (1993). Dynamics of fault interaction: Parallel strike-slip faults.
419 *Journal of Geophysical Research: Solid Earth*, *98*(B3), 4461–4472.
420 Harris, R. A., & Day, S. M. (1999). Dynamic 3D simulations of earthquakes on en echelon
421 faults. *Geophysical Research Letters*, *26*(14), 2089–2092.
422 Hunter, J. D. (2007). Matplotlib: A 2D graphics environment. *Computing in Science &*
423 *Engineering*, *9*(03), 90–95.
424 Ida, Y. (1972). Cohesive force across the tip of a longitudinal-shear crack and Griffith's specific
425 surface energy. *Journal of Geophysical Research*, *77*(20), 3796–3805.
426 Kaiser, A., Balfour, N., Fry, B., Holden, C., Litchfield, N., Gerstenberger, M., D'anastasio, E.,
427 Horspool, N., McVerry, G., Ristau, J., & others. (2017). The 2016 Kaikōura, New
428 Zealand, earthquake: Preliminary seismological report. *Seismological Research Letters*,
429 *88*(3), 727–739.
430 Kyriakopoulos, C., Wu, B., & Oglesby, D. D. (2021). Asymmetric topography causes normal
431 stress perturbations at the rupture front: The case of the Cajon Pass. *Geophysical*
432 *Research Letters*, e2021GL095397.
433 Liu, Z., & Duan, B. (2016). Coseismic slip gradient and rupture jumps on parallel strike-slip
434 faults. *Bulletin of the Seismological Society of America*, *106*(1), 204–212.
435 Lozos, J. C., Dieterich, J. H., & Oglesby, D. D. (2014). The Effects of d0 on Rupture
436 Propagation on Fault StepoversThe Effects of d0 on Rupture Propagation on Fault
437 Stepovers. *Bulletin of the Seismological Society of America*, *104*(4), 1947–1953.
438 Oglesby, D. (2008). Rupture termination and jump on parallel offset faults. *Bulletin of the*
439 *Seismological Society of America*, *98*(1), 440–447.
440 Oskin, M. E., Arrowsmith, J. R., Corona, A. H., Elliott, A. J., Fletcher, J. M., Fielding, E. J.,
441 Gold, P. O., Garcia, J. J. G., Hudnut, K. W., Liu-Zeng, J., & others. (2012). Near-field
442 deformation from the El Mayor–Cucapah earthquake revealed by differential LIDAR.
443 *Science*, *335*(6069), 702–705.

Ozalaybey, S., Ergin, M., Aktar, M., Tapirdamaz, C., Biçmen, F., & Yörük, A. (2002). The 1999 Izmit earthquake sequence in Turkey: Seismological and tectonic aspects. *Bulletin of the Seismological Society of America*, *92*(1), 376–386.

Ramos, M. D., Neo, J. C., Thakur, P., Huang, Y., & Wei, S. (2020). Stress Changes on the Garlock fault during and after the 2019 Ridgecrest Earthquake Sequence. *Bulletin of the Seismological Society of America*.

Ross, Z. E., Idini, B., Jia, Z., Stephenson, O. L., Zhong, M., Wang, X., Zhan, Z., Simons, M., Fielding, E. J., Yun, S.-H., & others. (2019). Hierarchical interlocked orthogonal faulting in the 2019 Ridgecrest earthquake sequence. *Science*, *366*(6463), 346–351.

Ryan, K. J., & Oglesby, D. D. (2014). Dynamically modeling fault step overs using various friction laws. *Journal of Geophysical Research: Solid Earth*, *119*(7), 5814–5829.

Shelly, D. R. (2020). A high-resolution seismic catalog for the initial 2019 Ridgecrest earthquake sequence: Foreshocks, aftershocks, and faulting complexity. *Seismological Research Letters*, *91*(4), 1971–1978.

Toda, S., & Stein, R. S. (2020). Long-and Short-Term Stress Interaction of the 2019 Ridgecrest Sequence and Coulomb-Based Earthquake Forecasts. *Bulletin of the Seismological Society of America*, *110*(4), 1765–1780.

Ulrich, T., Vater, S., Madden, E. H., Behrens, J., van Dinther, Y., Van Zelst, I., Fielding, E. J., Liang, C., & Gabriel, A.-A. (2019). Coupled, physics-based modeling reveals earthquake displacements are critical to the 2018 Palu, Sulawesi tsunami. *Pure and Applied Geophysics*, *176*(10), 4069–4109.

Wald, D. J., & Heaton, T. H. (1994). Spatial and temporal distribution of slip for the 1992 Landers, California, earthquake. *Bulletin of the Seismological Society of America*, *84*(3), 668-691 %@ 1943-3573.

Wang, H., Liu, M., Duan, B., & Cao, J. (2020). Rupture propagation along stepovers of strike-slip faults: Effects of initial stress and fault geometry. *Bulletin of the Seismological Society of America*, *110*(3), 1011–1024.

Wang, H., Liu, M., Ye, J., Cao, J., & Jing, Y. (2017). Strain partitioning and stress perturbation around stepovers and bends of strike-slip faults: Numerical results. *Tectonophysics*, *721*, 211–226.

Wesnousky, S. G. (1988). Seismological and structural evolution of strike-slip faults. *Nature*, *335*(6188), 340–343.

Wesnousky, S. G. (2006). Predicting the endpoints of earthquake ruptures. *Nature*, *444*(7117), 358–360.

Wollherr, S., Gabriel, A.-A., & Mai, P. M. (2019). Landers 1992 “reloaded”: Integrative dynamic earthquake rupture modeling. *Journal of Geophysical Research: Solid Earth*, *124*(7), 6666–6702.

Ye, J., Liu, M., & Wang, H. (2015). A numerical study of strike-slip bend formation with application to the Salton Sea pull-apart basin. *Geophysical Research Letters*, *42*(5), 1368–1374.

Zhang, Z., Xu, J., & Chen, X. (2016). The supershear effect of topography on rupture dynamics. *Geophysical Research Letters*, *43*(4), 1457–1463.

Acknowledgement

This research is partly supported by SCEC grant 22144. Figures in this manuscript were generated using GMT (Wessel and Smith, 1998), Matplotlib (Hunter, 2007) and Paraview (available from https://www.paraview.com). I used the software Cubit version 21.5 to mesh the finite element models and FaultMod to compute the physics of the dynamic rupture simulations. I thank David Oglesby and Baoning Wu for fruitful discussion that helped moved this project forward.

List of Tables

P and S wave velocity	5480 m/s; 3160 m/s
Density	2700 kg/m^3
Radius of nucleation zone	5000 m
Hexahedral Mesh size	200 m
Slip-weakening distance (d_0)	0.4 m; 0.3 m
Static friction (μ_s)	0.75
Dynamic friction (μ_d)	0.30
Initial shear stress (τ_0)	10 MPa
Initial normal stress (σ_n)	16.65 MPa
S value ($\frac{\mu_s * \sigma_n - \tau_o}{\tau_o - \mu_d * \sigma_n}$)	0.5

Table 1: Model and frictional parameters for the dynamic rupture simulations

List of Figures

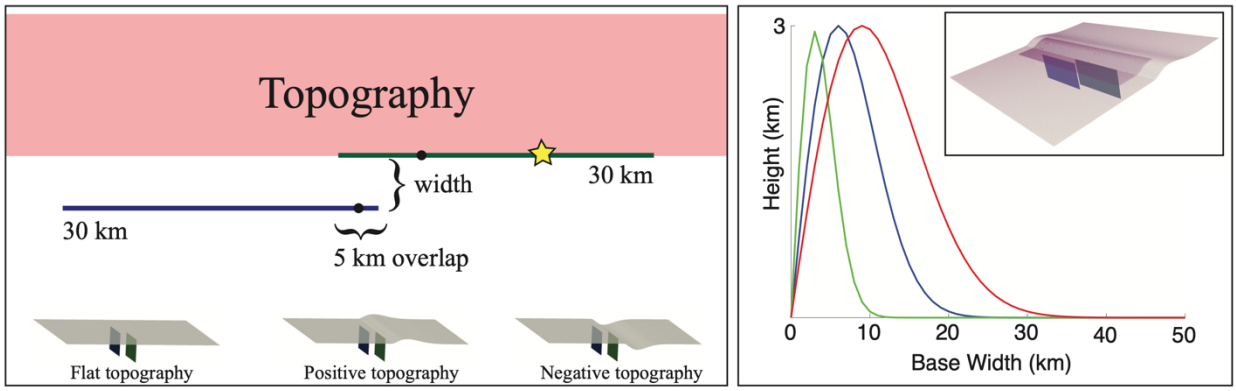

Figure 1: *The top part in the left panel shows the 2D sketch of the fault stepover configuration with the topography in map view. Fault 1 or ruptured fault is shown in green and fault 2 in blue. The red shaded area marks the position of topography (positive or negative). The yellow star shows the location of the nucleated point. The black dots mark the locations where I evaluate slip, shear and normal stresses time histories (see figure 5). The bottom part of the left panel shows the 3D views for the flat, positive, and negative topography cases. The right panel shows the 2D Rayleigh distribution of topography with respect to fault 1 located at the origin. The red, blue, and green distributions are for a base width of 30, 20 and 10 km respectively (see Figure 8). The inset in the right panel shows the finite element mesh.*

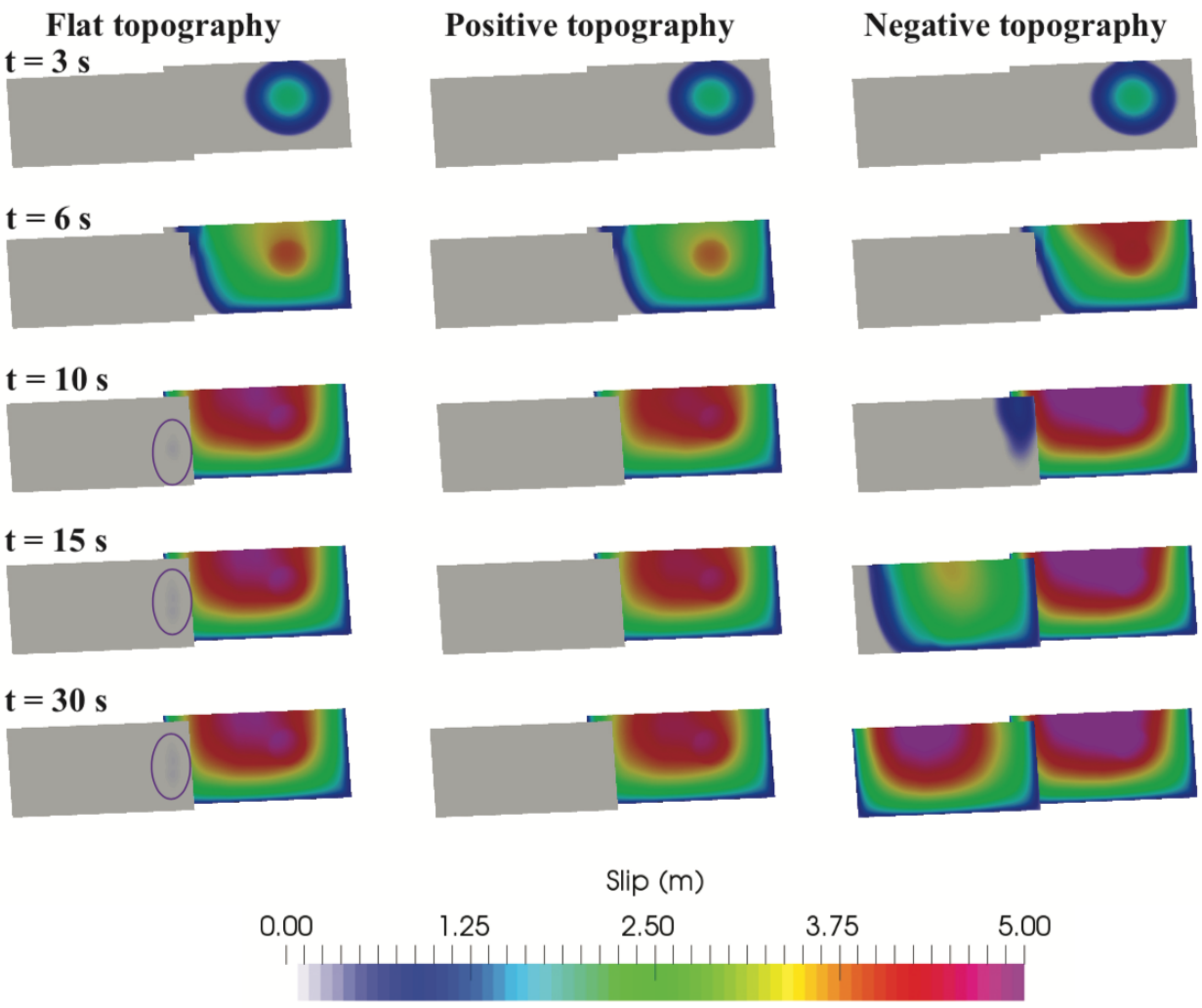

Figure 2: *Snapshots of the slip distribution at different time steps for the flat, positive and negative topography cases for a slip weakening distance of 0.4 m. The bottom row is the final slip distribution. The purple ellipse on the flat topography case marks the location where rupture triggers on the receiver fault but rapidly dies out.*

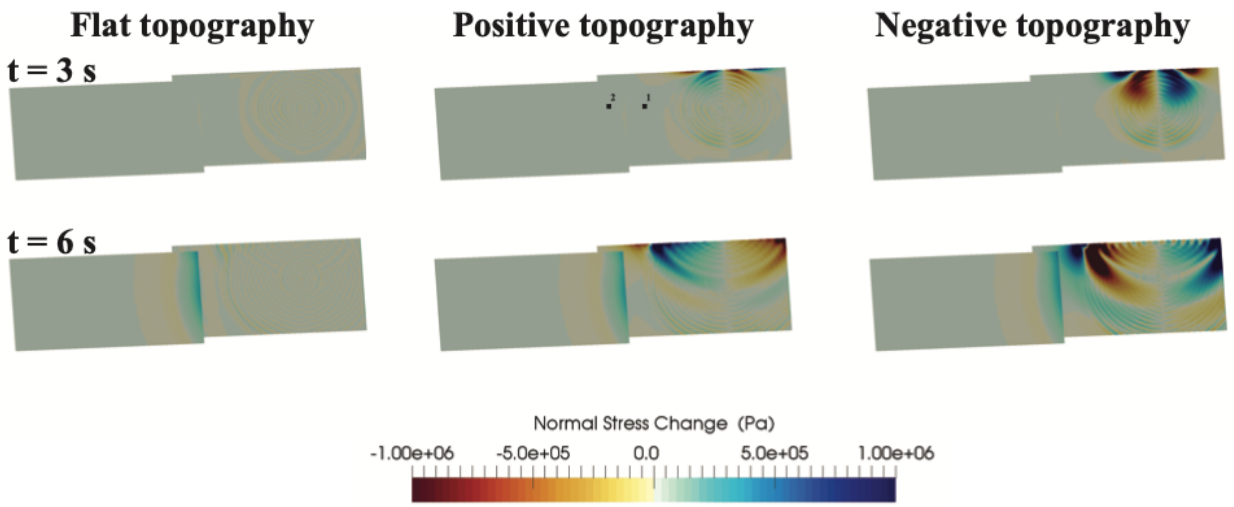

Figure 3: *Snapshots of the normal stress change at time steps 3 and 6 s for the flat, positive and negative topography cases. Blue color indicates a clamping effect and red an unclamping effect. The black dots 1 and 2 on fault 1 and fault 2 respectively mark locations where I evaluate slip, shear stress and normal stress time histories (see Figure 4). For this extensional stepover, a positive topography causes an increase of the normal stress behind the rupture front while a negative topography causes a decrease of the normal stress behind the rupture front.*

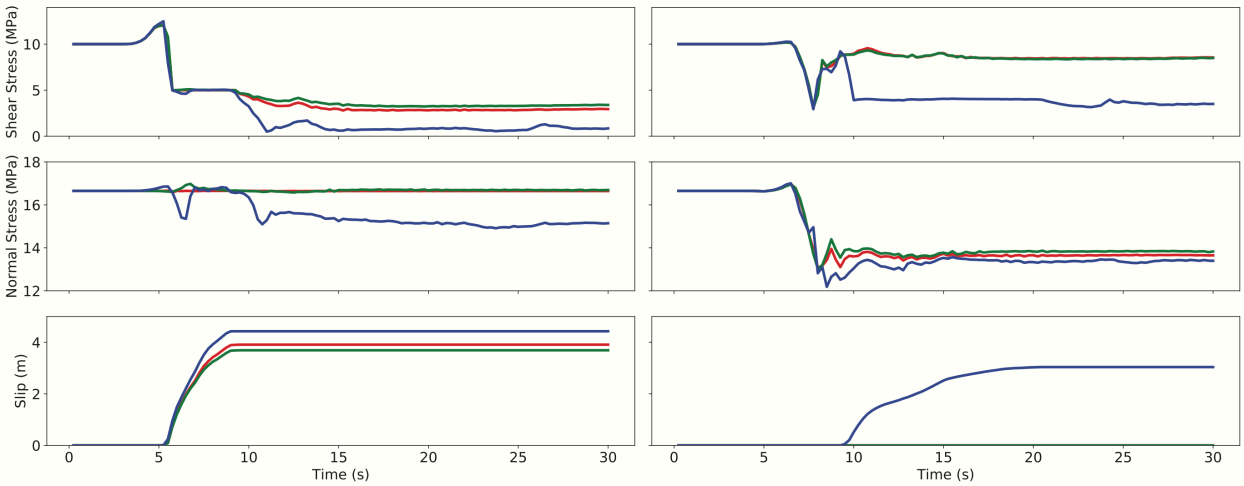

Figure 4: *Slip, normal stress and shear stress histories for point 1 on fault 1 (1st column) and point 2 on fault 2 (2nd column). The locations of those two points are shown in Figure 1. Red, green and blue lines show the result of the flat, positive and negative topography cases respectively for a slip-weakening distance of 0.4 m and a stepover width of 4 km.*

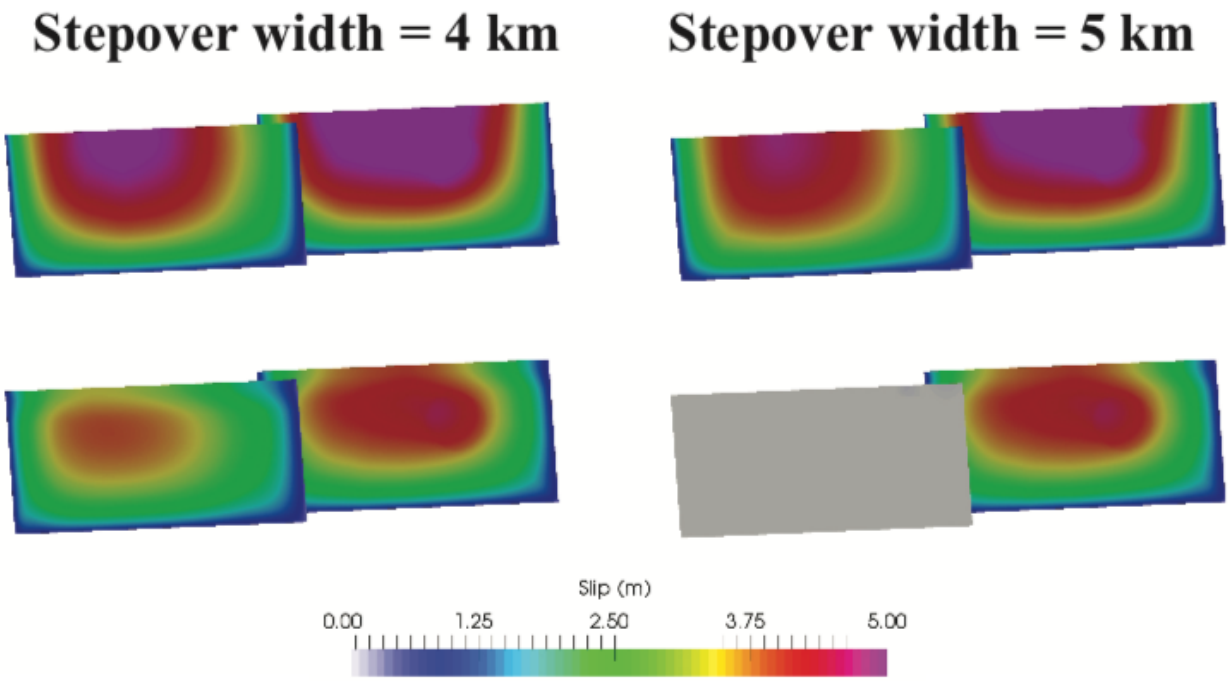

Figure 5: *Final slip distribution for the negative topography, for an extensional stepover width of 4 km (1st column) and 5 km (2nd column) and for a slip-weakening distance of 0.4 m. The upper row shows results for homogeneous stress conditions and the bottom row shows results where the shear and normal stresses are tapered linearly.*

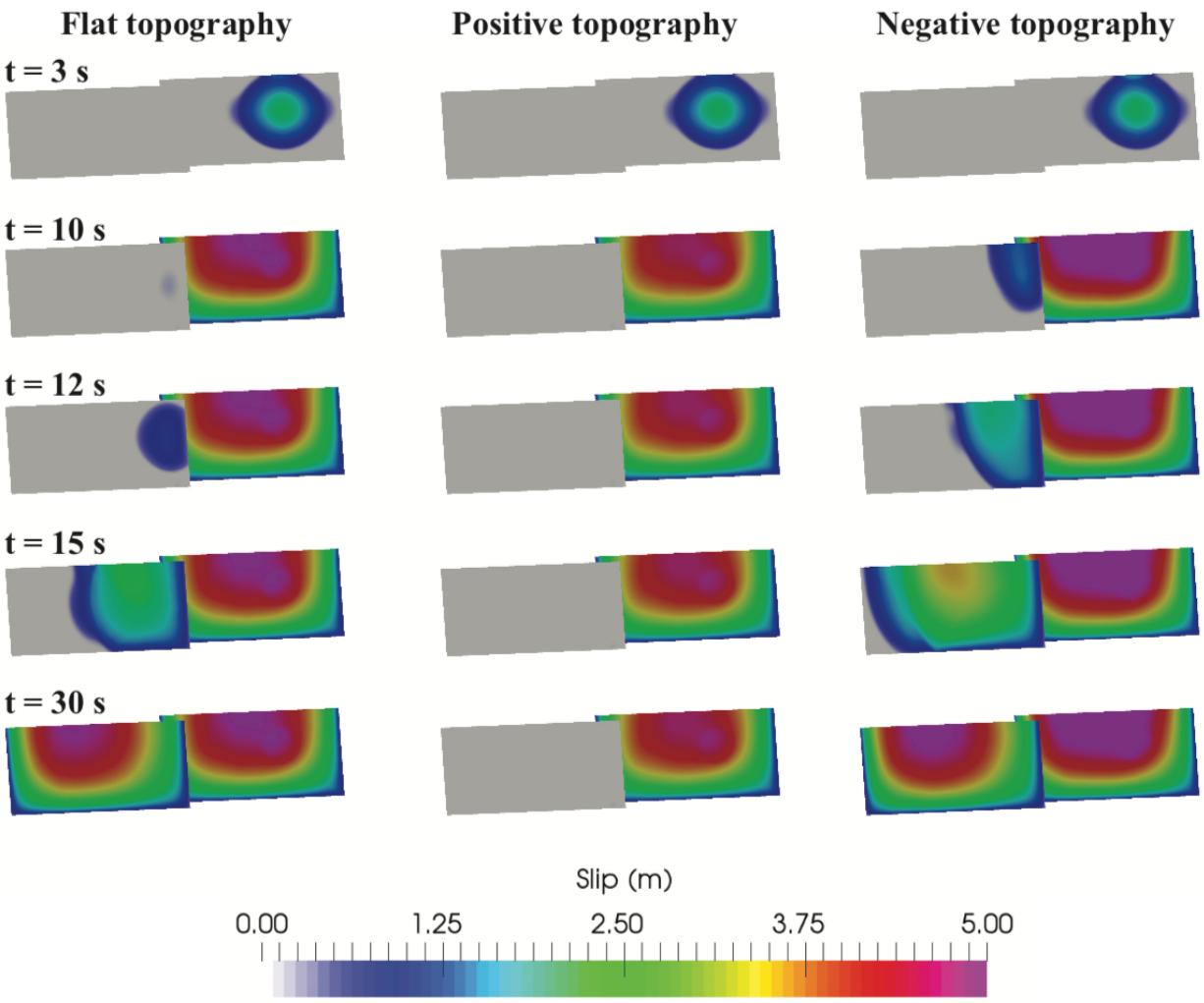

Figure 6: *Snapshots of the slip distribution at different time steps for the flat, positive and negative topography cases for a slip weakening distance of 0.3 m and stepover width of 4 km. The last line is the final slip distribution.*

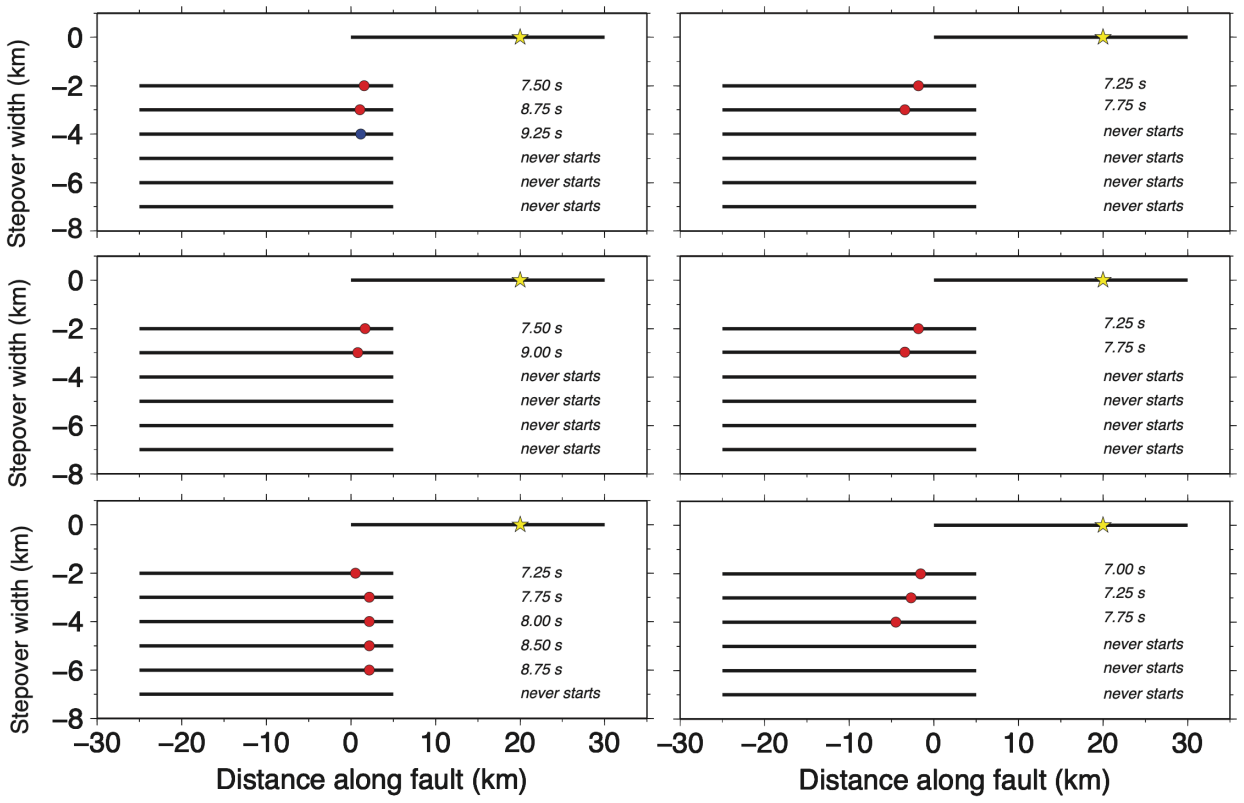

Figure 7: *Summary of rupture behavior for various stepover widths for the 0.4 m slip weakening case. The left column shows the extensional stepover (left-lateral strike-slip) and the right column the compressional stepover (right-lateral strike-slip. The top, middle and bottom panels are for a flat, positive and negative topography respectively. The yellow star marks the location of the nucleation point on fault 1. The circles show the locations of the initial triggering point on fault 2 and the time when rupture on fault 2 is triggered are shown on the right for each case. A red circle indicates that fault 2 breaks entirely while a blue circle indicates that rupture dies out on fault 2.*

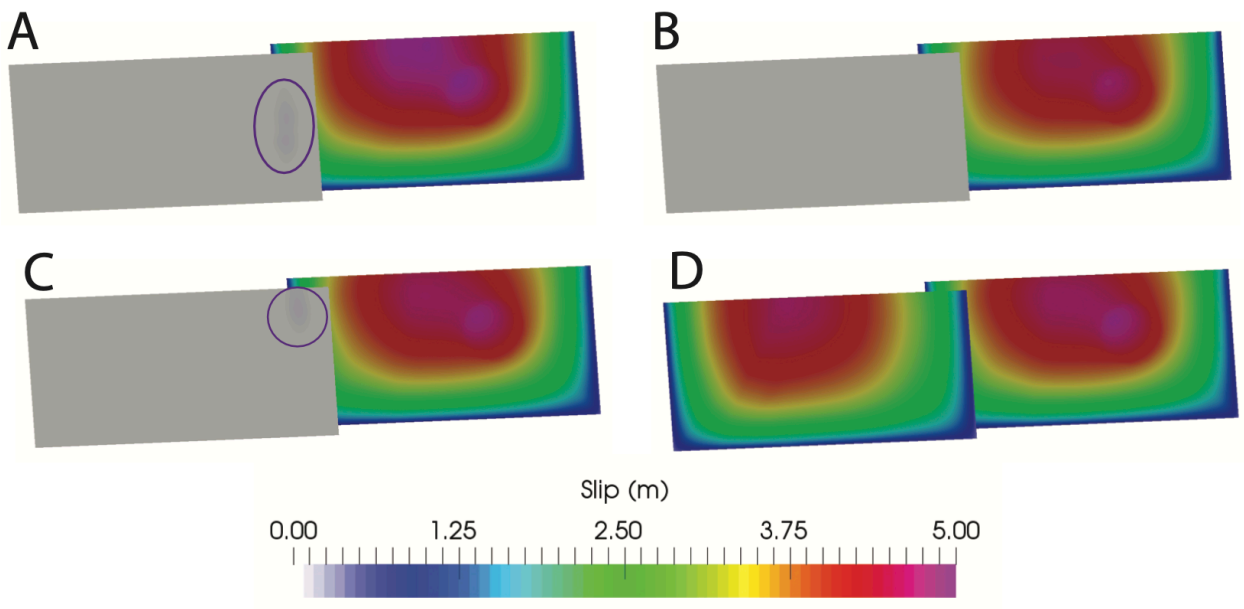

Figure 8: *Final slip on an extensional stepover width of 4 km with a slip-weakening distance of 0.4 m. Panel A marks the flat topography case, same as in Figure 2; panel B is for positive topography width of 30 km, same as in Figure 2; panel C is for a positive topography width of 20 km and panel D is for a positive topography width of 10 km.*

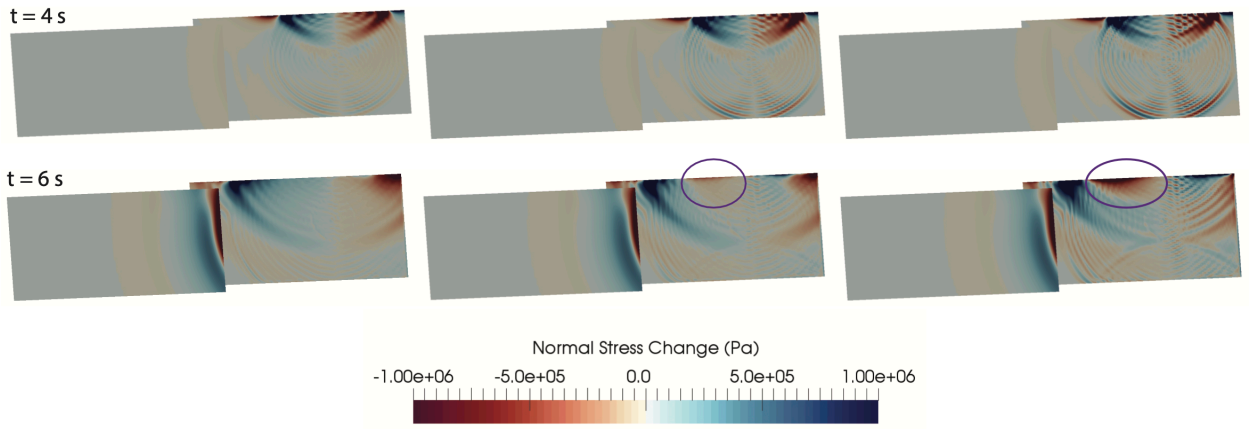

Figure 9: *Snapshots of the normal stress change at time steps 4 and 6 s for the positive topography width of 30 km (1st column, same as in Figure 4), 20 km (2nd column) and 10 km (3rd column). For this extensional stepover, positive topography causes an increase of the normal stress behind the rupture front followed by a decrease only for the narrower topography (20 and 10 km) as shown by the purple ellipse. This subsequent decrease of the normal stress can lead the rupture to jump across the extensional stepover.*

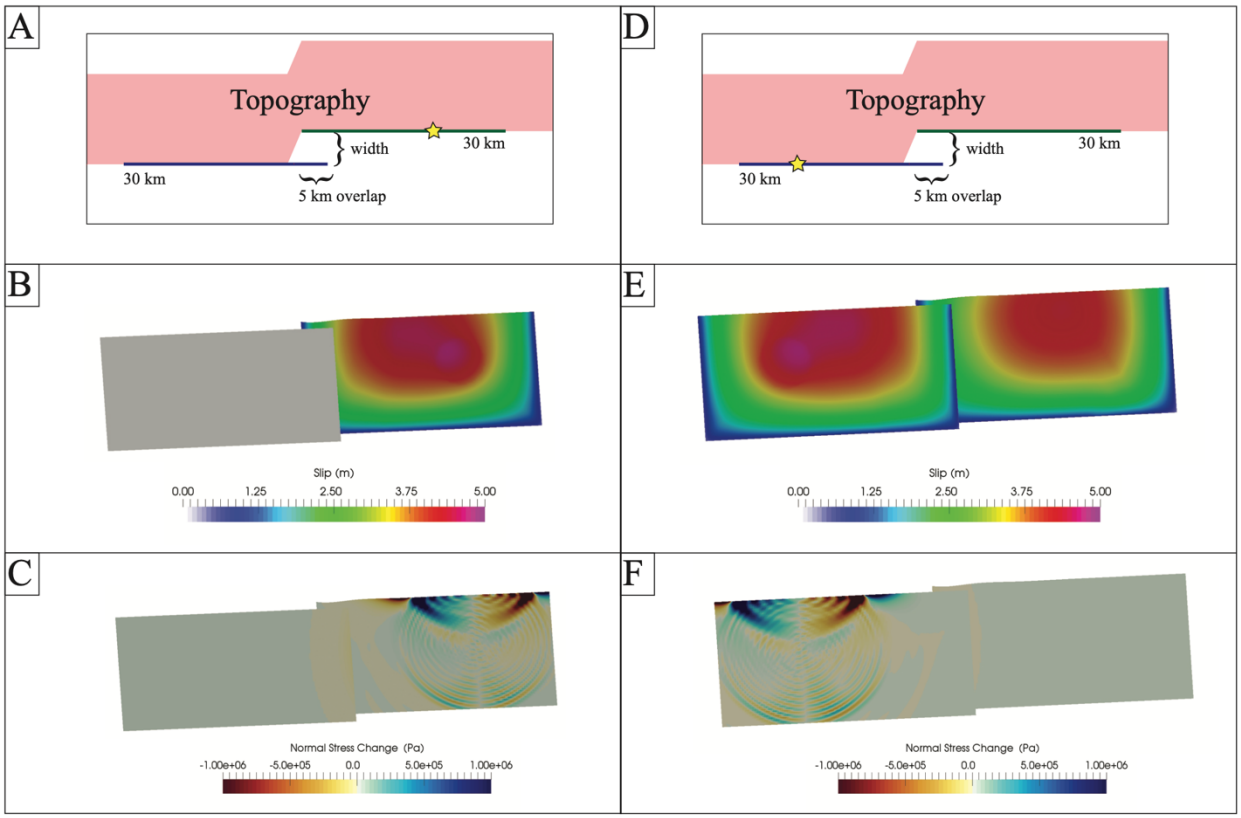

Figure 10: Left column shows the sketch and dynamic simulation for a rupture initiated on fault 1 and the right column is for a rupture initiated on fault 2. Panels A and D show the new 2D sketch of the fault stepover configuration with the position of the positive topography (red shaded area) in map view. The yellow star shows the location of the nucleated point. Panels B and E show the final slip on an extensional stepover width of 4 km with a slip-weakening distance of 0.4 m and panels C and F mark the snapshot of the normal stress change at 4 s. For the rupture initiated on fault 2, the decrease in normal stress behind the rupture front allows the rupture to propagate on fault 1.

Effect of Asymmetric Topography on Rupture Propagation along Fault Stepovers

Roby Douilly
University of California, Riverside

Corresponding author: Roby Douilly (roby.douilly@ucr.edu)

Key points:

- Asymmetric topography can affect rupture propagation across fault stepovers
- Topography can cause a clamping or unclamping effect that can prevent or facilitate a rupture to jump a wider extensional stepover
- With topography, changing the hypocenter location can have a significant impact on throughgoing rupture across fault stepovers.

Abstract:

Complex fault systems are often located in regions with asymmetric topography on one side of a fault, and these systems are very common in Southern California. Along these fault systems, geometrical complexities such as stepovers can impact fault rupture. Previous rupture dynamic studies have investigated the effect of stepover widths on throughgoing rupture, but these studies didn't examine the influence of topography on the rupture behavior. To investigate the effect of asymmetric topography on rupture dynamics at stepovers, I consider three cases: 1) a flat topography, 2) a positive (mountain) and 3) a negative (basin) topography on only one side of the fault system outside of the stepover. In each case, I use the 3D finite element method to compute the rupture dynamics of these fault systems. The results show a significant time dependent variation of the normal stress for the topography cases as opposed to the flat surface case, which can have an important impact on rupture propagation at the stepover. For a positive topography on the right of the rupture propagation, there is a clamping effect behind the rupture front that prevents the rupture to jump a wider extensional stepover. The opposite is observed for a negative topography or for a positive topography on the left side of the rupture propagation, where the rupture can jump over a wider compressional stepover. These results suggest that topography should be considered in dynamic studies with geometric complexities such as stepovers, and perhaps bends and branched fault systems.

Plain Language Summary:

Topography such as a mountain range or a basin can be found near faults across the world. This work investigates whether a surface topography can affect an earthquake to propagate across fault stepovers which are discontinuous faults with an offset of some distance with one another. I use three-dimensional dynamic models to generate a number of earthquake scenarios using different types of topography (mountain or basin). I find that the type of topography can sometimes prevent or facilitate an earthquake rupture to propagate across a fault stepover. While numerical experiment without topography has shown it is unlikely for an earthquake to propagate across a stepover width greater than 4 km, adding topography can cause the rupture to jump beyond 4 km. This result could be a potential explanation as to why some past earthquakes are able to jump a stepover width of 4 km or greater while others couldn't and it could have real hazard implications for future earthquakes on stepovers.

1. Introduction

Major earthquakes often involve multiple fault segments by propagating across geometric complexities such as fault stepover. One important example is the 1968 Borrego mountain earthquake (Wesnousky, 1988). During this event, the rupture was able to propagate across a 1.5 km restraining step but couldn't jump a releasing stepover of 7 km nor a restraining stepover of 2.5 km. Other more recent earthquakes such as the 1992 Landers earthquake (Wald & Heaton, 1994), the 1999 Izmit earthquake (Ozalaybey et al., 2002), and the 2019 Ridgecrest sequence (Ross et al., 2019) involved rupture propagating across fault stepovers, with the width of those jumped stepovers not exceeding 4 km. Understanding whether a rupture is likely to jump across a stepover during a single event is crucial, as it will affect the overall earthquake size. Wesnousky, (2006) analyzed surface traces of 22 historical strike-slip earthquakes and found that no events within that group were able to jump a width of 5 km or above. Furthermore, very few earthquakes were able to jump a stepover width of 3-4 km, and 40% of the events below that threshold also didn't propagate across. The Uniform California Earthquake Rupture Forecast 3 (UCERF3) seismic hazard analysis even incorporates a 5 km limit above which a single rupture cannot jump (Field et al., 2014). However, a few exceptional earthquakes have been observed where the rupture appeared to jump a step greater than 5 km. The 2010 El Mayor-Cucapah earthquake ruptured across a 120 km long multi-fault segments and the rupture appeared to propagate across a 10 km wide stepover with potentially intermediary sub-faults (Oskin et al., 2012). The 2016 Kaikoura New Zealand earthquake ruptured more than a dozen fault segments with apparent rupture jump stepovers greater than 15 km (Kaiser et al., 2017; Ulrich et al., 2019). Therefore, it is important to proper evaluate the factors that could limit or facilitate a rupture to jump across wide stepovers.

A number of numerical modeling studies have attempted to point out some key physical parameters (*i.e.* fault geometry, initial stress and frictional parameters) that could affect throughgoing rupture across stepovers. Fault geometry is clearly a major effect in rupture propagation. Harris et al., (1991) and Harris & Day, (1993) performed 2D dynamic models of a series of super-shear ruptures across strike-slip fault steps for various stepover widths (1-6 km). They found that the rupture could jump across both a restraining and releasing stepover, and argued that the rupture is unlikely to jump a releasing stepover wider than 5 km and restraining stepover wider than 2.5 km. The seismogenic depth of a fault is another controlling effect where rupture on a fault with large seismogenic depth can jump wider stepovers (Bai & Ampuero, 2017). Furthermore, the frictional properties could also affect rupture propagation. Ryan & Oglesby, (2014) argued that the likelihood for a rupture to jump large stepovers is dependent on the friction parameterization used where rate and state friction with strong rate-weakening can facilitate the rupture to jump over large stepovers (> 7km). Other studies have found that the choice of the slip-weakening distance can also affect throughgoing rupture across stepovers where increasing the slip-weakening distance can prevent a rupture from jumping across a stepover and vice-versa (Lozos et al., 2014). Moreover, Liu & Duan, (2016) argued that there is a linear relationship between the maximum jumpable stepover and the slip gradient where a larger stress drop will

facilitate the rupture to jump a wider stepover. Another key factor to consider is the heterogeneity in the state of stress particularly near the geometrical discontinuities. While homogeneous stress is usually assumed in previous dynamic rupture models, Duan & Oglesby, (2007) show that over multiple earthquake cycles, a heterogeneous fault stress field can develop near a fault branch due to the interactions of the different segments, and this could impact the ability of rupture to propagate across the stepover. Furthermore, significant stress variations are observed near stepovers due to long-term fault tectonics (Wang et al., 2017; Ye et al., 2015). Harris & Day, (1999) mentioned that heterogenous stress distribution can affect rupture where earthquakes occurring on faults close to failure, due to a prior rupture, may jump wider stepovers. More recently, Wang et al., (2020) use 2D dynamic rupture models to investigate the effect of heterogenous fault stress from long term simulation on fault stepovers. They argued that a rupture can jump up to 20 km across overlapping releasing stepovers and up to 7 km across restraining stepovers.

Some recent dynamic studies have started to incorporate surface topography in their modeling despite the increased level of complexity it poses (Ulrich et al., 2019; Wollherr et al., 2019). Adding topography involves technical challenges—it will not only make the volume more difficult to mesh, but it will require significantly more processing power and a longer computational time. Nevertheless, surface topography has been seen to cause noticeable fluctuations in rupture behavior for scenarios of earthquakes on a single fault segment. Zhang et al., (2016) modeled rupture dynamics on a fault with varying topographic surfaces and they argued that depending on the shape (hill or valley) and epicentral distance to the fault, topography can affect the sub-shear to super-shear transition. More recently, Kyriakopoulos et al., (2021) investigated the effect of asymmetric topography on a single fault and found that the position of the topography with respect to the rupture propagation can either cause a positive (clamping effect) or negative (unclamping effect) normal stress perturbation behind the rupture front and an opposite normal stress effect ahead of the rupture front. In addition, most major fault systems tend to be located in region with asymmetric topography. This type of asymmetric topography next to a fault system can be seen at several location around southern California. As an example, mountain ranges can be seen primarily between the fault segmentation that ruptured during the 2010 El Mayor-Cucapah earthquake (Oskin et al., 2012). Also, the left-lateral Garlock fault system, which is composed of two segments separated by an extensional stepover width of 3-4 km, has high mountain ranges on its northern side and almost a flat topography on the southern side. This stepover is particularly important because the recent 2019 Ridgecrest sequence triggered significant seismicity on the Garlock fault (Cochran et al., 2020; Shelly, 2020) and an important increase in shear stress was also observed on that segment near the segmentation (Ramos et al., 2020). Considering that the aforementioned stepover modeling studies assumed a flat topography and didn't explore whether surfaces with irregular topographies can also impact rupture propagation across fault segmentation, it is worth investigating whether topography can also affect rupture jump across fault stepovers.

Here I use 3-D dynamic rupture simulations to investigate if mountain ranges (positive topography) or valleys (negative topography) can facilitate or hinder a rupture from propagating across a vertical strike-slip fault stepover. I will vary the position and shape of the geometry with respect to the stepover to understand which details of the model have controlling effects on rupture behavior.

2. Model setup and computational parameters

The main objective of this study is to highlight the effects asymmetric topography can have on fault segmentation. I consider the stepover to be composed of two vertical planar fault segments (fault 1 and fault 2) of 30 km each with 15 km locking depth and with a 5 km overlap. I explore offsets or stepover widths that vary from 2 to 8 km. A synthetic topography with a Rayleigh distribution (Figure 1) is added on the northern portion of the stepover so that the fault system has no elevation (the fault system is on the free surface at 0 km) and the topography is distributed over a 30 km horizontal distance perpendicular to strike (Figure 1). For each geometry, I consider three different types of topography: 1) a no topography case which will serve as a comparison to other dynamic model studies (*e.g.*, Harris et al., 1991; Harris & Day, 1993), 2) a positive topography case (or mountain range) and 3) a negative topography case (or valley). For all geometries, we build a three-dimensional finite element mesh using the Cubit software version 2021.5, with the model space discretized with hexahedral elements of 200 m size within and around the volume hosting the faults, but becoming coarser (800 m) away from the fault system (see inset in Figure 1).

The meshes are then imported into the 3-D finite element code FaultMod (Barall, 2009), which has been validated through the Southern California Earthquake Data Center community rupture verification code (Harris et al., 2009; 2018). To implement the dynamic rupture models, I consider a uniform pre-stress conditions (Table 1) with strength parameter (S) of 0.5, which leads to super-shear rupture similar to the modeling studies of Harris & Day, (1993). The S value is the ratio between the strength excess (yield stress minus initial stress) and the dynamic stress drop (initial shear stress minus sliding stress) as defined by Das & Aki, (1977). I implement the stress conditions so that the faults have a left-lateral strike-slip motion consistent with the releasing stepover on the Garlock fault, but for completeness I also test scenarios for a restraining stepover (or a right-lateral strike-slip motion) on the faults. The friction law used in this study is the linear slip-weakening (Andrews, 1976; Ida, 1972) where I assume a slip-weakening distance, static friction and dynamic friction of 0.4 m, 0.75 and 0.3 respectively. However, since Lozos et al. (2014) inferred that decreasing the slip-weakening distance could facilitate the rupture to jump across a wider stepover (Lozos et al., 2014), I also test cases with slip-weakening distance of 0.3 m. Table 1 summarizes the values of all the computational parameters for the rupture simulations conducted in this study.

3. Results

For each scenario, I nucleate the rupture at the same location on fault 1 (green fault in Figure 1) by creating a circular region in which the shear stress is 10% greater than the failure stress so that the nucleation zone ruptures instantaneously and analyze whether topography affects the rupture behavior on both fault (fault 1 and fault 2) of the stepover system. In the following, the nucleated segment will be referred to as source fault and the other segment of the stepover as receiver fault. Figure 2 shows the evolution of slip for the three geometries (flat, positive, and negative topographies) with a releasing stepover width of 4 km and for a slip-weakening distance of 0.4 m. On the source fault (fault 1 in this case), the type of topography does not change the rupture speed, but it does affect the total slip. With a topography on the right of the rupture propagation for a left-lateral strike-slip fault (releasing stepover), a positive topography causes less slip to develop on the source fault as opposed to the flat case. On the other hand, more slip is observed for the negative topography compared to the flat case. Furthermore, adding topography affects the ability for a rupture to jump across the stepover. For the flat topography case and for a slip-weakening distance of 0.4 m, the rupture jumps across the stepover and triggers small slip on the receiver fault (purple ellipse in Figure 2), but the rupture rapidly dies out. However, a positive topography prevents the rupture from jumping across, while a negative topography facilitates the rupture to jump, and the rupture breaks the receiver fault in its entirety.

Kyriakopoulos et al. (2021) investigated the impact of asymmetric topography along a single vertical fault, and they showed that with topography on the right of propagating rupture for a right lateral strike-slip fault, there is clamping (increase of normal stress) ahead of the rupture front and unclamping (decrease of normal stress) behind the rupture front; the effect reverses when the mountains are on the opposite side of the fault. I also observe these normal stress perturbations, and they affect rupture propagation across a fault stepover. Figure 3 shows the normal stress change at sequential time steps for the three topographic cases (flat, positive, and negative topography) on the releasing stepover. For the flat topography, there is no significant normal stress perturbation. For a positive topography on the right of the rupture propagation for left-lateral strike-slip fault, there is a decrease in normal stress (unclamping) ahead of the rupture front and an increase in normal (clamping) stress behind the rupture front, consistent with Kyriakopoulos et al. (2021). The opposite is observed for the negative topography, where there is an unclamping behind the rupture front a clamping ahead of the rupture front. These perturbations cause fluctuations in normal stress on the receiver fault. Figure 4 shows the time evolution of slip, shear stress and normal stress on points on fault 1 and fault 2 as located in Figure 3. The topography induced normal stress perturbation behind the rupture front on the source fault is much larger compared to the one ahead of the rupture, and is the leading factor to affect rupture propagation. For the negative topography, the unclamping effect behind the rupture front on fault 1 induces a decrease in normal stress on fault 2 on top of the overall normal stress decrease caused by the extensional stepover. This additional decrease causes the shear stress to overcome the failure stress and thus triggers slip on fault 2. On the other hand, the clamping effect behind the rupture front

for the positive topography case on the right side of the rupture propagation for a releasing stepover causes a normal stress increase on fault 2 that pushes the fault further away from failure. Therefore, the addition of topography can significantly alter the outcome of a rupture propagation across a stepover.

Another important observation is that the addition of topography affects the peak slip near the free surface. Amplified slip near the free surface causes the rupture to trigger the receiver fault near the surface instead of at depth as it is for the flat case. This is most likely due to the fact that the topographically-induced normal stress perturbations are higher near the surface and decrease with depth, also consistent with Kyriakopoulos et al. (2021) (Figure 3). To further explore this issue, I consider scenarios using the same frictional conditions as in Figure 2 (slip-weakening distance of 0.4 m) but in addition, I linearly taper the shear and normal stresses in the upper 3 km. Figure 5 and supplemental video 1 show the final slip for the negative topography case for releasing stepover widths of 4 km and 5 km with non-tapered (upper panels) and tapered (lower panels) initial stress conditions. Similar to the fully homogeneous stress cases, ruptures are still being triggered close to the free surface and not at depth as it is for the flat topography case. It is worth noting that increasing the gap not only causes a decrease of the maximum slip on the receiver fault but also leads to a delay triggering of the receiver fault. However, tapering the stresses in the upper few kilometers does limit throughgoing rupture across wider step over since less slip develops on both faults. Despite the decrease in the maximum slip, the rupture was able to jump across the releasing stepover for a 4 km gap but couldn't propagate a stepover width of 5 km. Considering Lozos et al., (2014) pointed out for the flat topography case that decreasing the slip-weakening distance does facilitate the rupture to jump a wider stepover, I also explore scenarios for a reduced slip-weakening distance value. I re-run the models described above by decreasing the slip-weakening distance from 0.4 m to 0.3 m for all three types of topography for stepover width of 4 km. For the flat case topography, decreasing the slip-weakening does allow the rupture to easily propagate across the stepover (Figure 6; supplemental video 2). However, a positive topography north of the fault system still prevents a throughgoing rupture across this releasing stepover. Topography also affects the triggering time on the receiver fault (fault 2). As shown in Figure 6, a negative topography north of the releasing stepover causes an early triggering of the receiver fault compared to the flat topography case.

4. Discussion

4.1. Impact of stepover gap and type of topography on throughgoing rupture

The rupture simulations described above show that topography (positive or negative) can affect rupture jumping across a stepover width of 4 or 5 km. But while there have been few real-world observations of such jumps, there have been some past earthquakes where the rupture appeared to jump a step greater than 4 km (Oskin et al., 2012; Ulrich et al., 2019). Previous dynamic modeling studies have shown that parameters such as slip-weakening distance (Lozos et al., 2014), friction law (Ryan et al., 2014), stress heterogeneity (Wang et al., 2020), seismogenic depth (Bai and

Ampuero, 2017), pore pressure (Liu and Duan, 2014) and slip gradient (Liu & Duan, 2016; Oglesby, 2008) can enable rupture to jump wider stepovers. To further investigate the impact of topography on stepover width, I generate more scenarios with stepover widths that vary from 2 to 8 km for a slip-weakening distance of 0.4 m. A detailed summary of the rupture behavior for various stepover widths is shown in Figure 7. In this analysis, a triggering time is considered when the slip rate on the receiver fault reaches a value of 0.1 m/s. For the flat case, the result is consistent with Harris and Day, (1999) which argued that a rupture rarely jumps across wide stepovers. Overall, a negative topography allows the rupture to jump across a wider stepover (max 6 km for an extensional stepover – see supplemental video 3) and it also causes an early triggering on the receiver fault as opposed to the flat and positive topography.

Adding a positive topography or mountain ranges can significantly alter rupture behavior across a fault stepover. In all the previous simulations, we assumed a fixed topography base width of 30 km that is distributed away from fault 1. Considering mountain ranges can be wide or narrow near a fault system, it is worth understanding whether a decrease of the base width would have any effect. Therefore, I consider 2 more scenarios with a base width of 20 km and 10 km respectively (see Figure 1). Figure 8 shows the final slip for the flat case (panel A), the positive topography with 30 km base width (panel B, same as in Figure 2), the positive topography with 20 km base width (panel C) and the positive topography with 10 km base width (panel D). While a wide base width prevents the rupture from jumping across the stepover for a rupture initiated on fault 1, decreasing the base width facilitates a throughgoing rupture (Supplemental video 4 and panel D in Figure 8). Figure 9 shows the normal stress changes at two different timestep for the cases shown in Figure 8. As shown above, a positive topography on the right side of the rupture propagation cause a clamping effect behind the rupture front for a releasing stepover that prevents the rupture from jumping across the stepover. However, for a positive topography distributed over a narrower distance (base width in the order of 10-20 km), following the clamping phase, there is a delayed unclamping effect (purple ellipse in Figure 9). For the base topography width of 20 km, the delayed unclamping phase is enough to facilitate the triggering of the receiver fault (fault 2) but the rupture rapidly dies out. Moreover, for the base width of 10 km, the trailing decrease in normal stress facilitates the rupture to jump across the extensional stepover and ruptures fault 2 entirely. Kyriakopoulos et al., (2021) argued that these dynamic normal stress perturbations are analogous to the normal stress change thrust faults cause inside and outside the slipping region. Therefore, I could argue that while a positive slope for the mountain side closest to the fault system does induce a clamping effect when the positive topography is on the right side of the rupture propagation, the negative side of the mountain side, which is further away from the system, would cause an opposite effect (unclamping) as shown in the Figure 9. Therefore, for a wider topography base width, I hypothesize that the delayed dynamic phases (Figure 9) are most likely attenuated with distance, which would explain why those delayed phases are not seen for the 30 km base width. This would suggest that these dynamic normal stress changes are dependent on the distance of the topography

to the fault system and thus topography that is far away from a fault system is unlikely to induce any normal stress perturbation.

4.2. Rupture behavior impacted by slip motion and hypocenter location

Ruptures on extensional stepovers are more prone to throughgoing rupture and are more likely to jump wider gap compared to ruptures on compressional stepovers (Harris et al., 1991; Harris and Day, 1993; Wang et al., 2020). Considering for an extensional stepovers, a positive topography on the right side of the rupture propagation causes a clamping effect behind the rupture front that can prevent throughgoing rupture, a compressional stepover (reversal of the slip direction or changing the system from a left-lateral to a right-lateral strike-slip) with those same conditions will cause the opposite effect (unclamping) behind the rupture front and thus could potentially facilitate the rupture to jump across. Therefore, I generate more rupture simulations across a restraining stepover for a range of stepover widths (2nd column of Figure 7). For a slip-weakening distance of 0.4 m, a rupture on a compressional stepover couldn't jump a stepover width of 4 km for both the flat and positive topography. However, when I decrease the slip-weakening distance from 0.4 m to 0.3 m, a positive topography on the right side of the rupture propagation still prevents a rupture from propagating across a releasing stepover width of 4 km, while numerical experiment shows that the rupture could easily jump across this stepover for the positive topography on a restraining stepover (Supplemental video 2). This is most likely due to the fact that positive topography on the right side of a restraining stepover (reversal of the slip direction) causes an unclamping behind the rupture as opposed to a clamping effect for the releasing stepover. However, unlike our previous scenarios where the triggering takes place within the overlapping region, for the restraining stepover, the rupture not only triggers at a distance outside the overlapping region but also an early triggering is observed on the receiver fault compare to the releasing stepover case (Figure 7). While the throughgoing rupture across the restraining stepover occurred because of the positive topography, the location of the triggering on the receiver fault is not associated with the topography. Harris et al., (1991) and Harris and Day, (1993) reported that releasing steps trigger later than restraining step and the initial point of rupture on the receiver fault is located away from the overlapping region. Furthermore, consistently with Harris et al., 1991 and Harris and Day, 1993, the bigger the width of the restraining stepover, the greater the triggering distance.

For all the scenarios above, I assume the same hypocenter location on fault 1. For the flat topography case, since the segments are planar and the initial stress conditions are homogeneous, the rupture pattern would be the same whether the hypocenter is on fault 1 or fault 2. However, considering that the dynamic normal stress fluctuations induced by the addition of topography vary with respect to the direction of the rupture propagation, moving the hypocenter to the other fault for the topography cases should lead to very different rupture behaviors. Therefore, I modified the geometry shown in Figure 1 (see Figures 10A and 10D) so that the positive topography follows the fault system across the stepover, staying close to fault 2 (instead of at a distance as it is in

Figure 1), considering that the induced normal stress perturbations attenuate if the topography is distant from the fault system. Figure 10E shows the final slip for a rupture initiated on fault 2 with a releasing stepover width of 4 km and for a slip-weakening distance of 0.4 m. While a rupture nucleated on fault 1 couldn't propagate all the way through the stepover for the positive topography case (Figure 10B and supplemental video 5), a rupture nucleated on fault 2 propagates very easily across the stepover. This is because for a rupture initiated on fault 2, the positive topography is on the left side of the rupture propagation and thus the normal stress perturbations are reversed compared to the cases in which the positive topography is on the right side. In particular, this shift causes a decrease in normal stress behind the rupture front that facilitates the rupture to jump across to fault 1 (Figure 10F). With the addition of topography alone, the location of the hypocenter either hinders or facilitates a rupture to propagate across a stepover. Therefore, this observation could be a potential explanation as to why some past earthquakes are able to jump a stepover width of 4 km or greater while others couldn't. Furthermore, this result has real hazard implications for future earthquakes on stepovers such as the one along the Garlock fault system. This would suggest that it is more likely for a rupture initiated on the Garlock fault close to the Ridgecrest region to stop at the stepover than a rupture initiated on the Garlock fault close to the San Andreas junction.

5. Conclusion

In this study, I used 3D dynamic rupture simulation to investigate the effect of topography on rupture propagation across releasing and restraining stepover. I consider three cases (flat topography, positive topography and negative topography) and assume a homogeneous stress conditions with a S value of 0.5. I find that asymmetric topography has a significant impact in influencing throughgoing rupture across fault stepovers. For a positive topography on the right of the rupture propagation for a left-lateral fault, there is clamping effect behind the rupture front that prevents the rupture to jump a wider extensional stepover. On the other hand, for a negative topography, an unclamping effect is observed behind the rupture front that facilitate the rupture to jump across a wider extensional stepover. While positive topography can hinder a rupture from propagating across a releasing stepover, rupture can easily jump across for the positive topography on a restraining stepover for a slip-weakening distance of 0.3 m and a stepover width of 4 km.

We can also observe that the topography doesn't change the rupture speed on the source fault, but it does affect the triggering time on the receiver fault. A negative topography on the north of the releasing stepover causes an early triggering of the receiver fault relative to a flat model. The topography base width can also affect through-going rupture. Although positive topography (on the right side of the rupture propagation) distributed over a wider distance can prevent a rupture from jumping across a releasing stepover, decreasing the base width of the topography (i.e., a narrower mountain range) can facilitate the rupture jumping across the stepover. Furthermore, changing the hypocenter location to fault 2 for the positive topography case will cause an unclamping effect behind the rupture front that can facilitate the rupture to jump across the stepover.

These results have strong implications for real case such as the 4 km gap releasing stepover on the eastern Garlock fault system, which has a positive topography north of the system that is distributed over a larger distance. My results would imply that it is less likely for a rupture initiated on the Garlock segment close to the Ridgecrest region to jump across this stepover due to the topography but more likely for a throughgoing rupture to occur if the rupture is initiated close to the San Andreas fault. However, I have to point out that the current models don't take into account factors such as depth dependent stresses (Aochi & Tsuda, 2023), stress heterogeneity (Douilly et al., 2020; Duan & Oglesby, 2007; Wang et al., 2020) and off-fault plasticity (Gabriel et al., 2013) that could also affect the likelihood of throughgoing rupture. This is particularly important considering that the 2019 Ridgecrest caused an increase in stress on the Garlock fault segment near the segmentation (Ramos et al., 2020). In addition, Toda & Stein, (2020) showed an increase in Coulomb stress change on the section of the Garlock fault closer to the San Andreas fault. Therefore, future studies that include heterogeneous shear stress, depth dependent normal stress and off-fault plasticity should be considered to further investigate the impact of topography on fault stepovers. Moreover, considering how topography can either hinder or facilitate rupture, future studies should also investigate whether topography has similar effect on other geometrical discontinuities such as branch fault system with variable dip angles.

References

Andrews, D. (1976). Rupture propagation with finite stress in antiplane strain. *Journal of Geophysical Research*, *81*(20), 3575–3582.

Aochi, H., & Tsuda, K. (2023). Dynamic rupture simulations based on depth-dependent stress accumulation. *Geophysical Journal International*, *233*(1), 182–194.

Bai, K., & Ampuero, J.-P. (2017). Effect of seismogenic depth and background stress on physical limits of earthquake rupture across fault step overs. *Journal of Geophysical Research: Solid Earth*, *122*(12), 10–280.

Barall, M. (2009). A grid-doubling finite-element technique for calculating dynamic three-dimensional spontaneous rupture on an earthquake fault. *Geophysical Journal International*, *178*(2), 845–859.

Cochran, E. S., Wolin, E., McNamara, D. E., Yong, A., Wilson, D., Alvarez, M., van der Elst, N., McClain, A., & Steidl, J. (2020). The US Geological Survey's rapid seismic array deployment for the 2019 Ridgecrest earthquake sequence. *Seismological Research Letters*.

Das, S., & Aki, K. (1977). A numerical study of two-dimensional spontaneous rupture propagation. *Geophysical Journal International*, *50*(3), 643–668.

Douilly, R., Oglesby, D. D., Cooke, M. L., & Hatch, J. L. (2020). Dynamic models of earthquake rupture along branch faults of the eastern San Gorgonio Pass region in California using complex fault structure. *Geosphere*, *16*(2), 474–489.

405 Duan, B., & Oglesby, D. D. (2007). Nonuniform prestress from prior earthquakes and the effect
406 on dynamics of branched fault systems. *Journal of Geophysical Research: Solid Earth*,
407 *112*(B5).
408 Field, E. H., Arrowsmith, R. J., Biasi, G. P., Bird, P., Dawson, T. E., Felzer, K. R., Jackson, D.
409 D., Johnson, K. M., Jordan, T. H., Madden, C., & others. (2014). Uniform California
410 earthquake rupture forecast, version 3 (UCERF3)—The time-independent model. *Bulletin*
411 *of the Seismological Society of America*, *104*(3), 1122–1180.
412 Gabriel, A.-A., Ampuero, J.-P., Dalguer, L., & Mai, P. M. (2013). Source properties of dynamic
413 rupture pulses with off-fault plasticity. *Journal of Geophysical Research: Solid Earth*,
414 *118*(8), 4117–4126.
415 Harris, R. A., Archuleta, R. J., & Day, S. M. (1991). Fault steps and the dynamic rupture
416 process: 2-D numerical simulations of a spontaneously propagating shear fracture.
417 *Geophysical Research Letters*, *18*(5), 893–896.
418 Harris, R. A., & Day, S. M. (1993). Dynamics of fault interaction: Parallel strike-slip faults.
419 *Journal of Geophysical Research: Solid Earth*, *98*(B3), 4461–4472.
420 Harris, R. A., & Day, S. M. (1999). Dynamic 3D simulations of earthquakes on en echelon
421 faults. *Geophysical Research Letters*, *26*(14), 2089–2092.
422 Hunter, J. D. (2007). Matplotlib: A 2D graphics environment. *Computing in Science &*
423 *Engineering*, *9*(03), 90–95.
424 Ida, Y. (1972). Cohesive force across the tip of a longitudinal-shear crack and Griffith's specific
425 surface energy. *Journal of Geophysical Research*, *77*(20), 3796–3805.
426 Kaiser, A., Balfour, N., Fry, B., Holden, C., Litchfield, N., Gerstenberger, M., D'anastasio, E.,
427 Horspool, N., McVerry, G., Ristau, J., & others. (2017). The 2016 Kaikōura, New
428 Zealand, earthquake: Preliminary seismological report. *Seismological Research Letters*,
429 *88*(3), 727–739.
430 Kyriakopoulos, C., Wu, B., & Oglesby, D. D. (2021). Asymmetric topography causes normal
431 stress perturbations at the rupture front: The case of the Cajon Pass. *Geophysical*
432 *Research Letters*, e2021GL095397.
433 Liu, Z., & Duan, B. (2016). Coseismic slip gradient and rupture jumps on parallel strike-slip
434 faults. *Bulletin of the Seismological Society of America*, *106*(1), 204–212.
435 Lozos, J. C., Dieterich, J. H., & Oglesby, D. D. (2014). The Effects of d0 on Rupture
436 Propagation on Fault StepoversThe Effects of d0 on Rupture Propagation on Fault
437 Stepovers. *Bulletin of the Seismological Society of America*, *104*(4), 1947–1953.
438 Oglesby, D. (2008). Rupture termination and jump on parallel offset faults. *Bulletin of the*
439 *Seismological Society of America*, *98*(1), 440–447.
440 Oskin, M. E., Arrowsmith, J. R., Corona, A. H., Elliott, A. J., Fletcher, J. M., Fielding, E. J.,
441 Gold, P. O., Garcia, J. J. G., Hudnut, K. W., Liu-Zeng, J., & others. (2012). Near-field
442 deformation from the El Mayor–Cucapah earthquake revealed by differential LIDAR.
443 *Science*, *335*(6069), 702–705.

Ozalaybey, S., Ergin, M., Aktar, M., Tapirdamaz, C., Biçmen, F., & Yörük, A. (2002). The 1999 Izmit earthquake sequence in Turkey: Seismological and tectonic aspects. *Bulletin of the Seismological Society of America*, *92*(1), 376–386.

Ramos, M. D., Neo, J. C., Thakur, P., Huang, Y., & Wei, S. (2020). Stress Changes on the Garlock fault during and after the 2019 Ridgecrest Earthquake Sequence. *Bulletin of the Seismological Society of America*.

Ross, Z. E., Idini, B., Jia, Z., Stephenson, O. L., Zhong, M., Wang, X., Zhan, Z., Simons, M., Fielding, E. J., Yun, S.-H., & others. (2019). Hierarchical interlocked orthogonal faulting in the 2019 Ridgecrest earthquake sequence. *Science*, *366*(6463), 346–351.

Ryan, K. J., & Oglesby, D. D. (2014). Dynamically modeling fault step overs using various friction laws. *Journal of Geophysical Research: Solid Earth*, *119*(7), 5814–5829.

Shelly, D. R. (2020). A high-resolution seismic catalog for the initial 2019 Ridgecrest earthquake sequence: Foreshocks, aftershocks, and faulting complexity. *Seismological Research Letters*, *91*(4), 1971–1978.

Toda, S., & Stein, R. S. (2020). Long-and Short-Term Stress Interaction of the 2019 Ridgecrest Sequence and Coulomb-Based Earthquake Forecasts. *Bulletin of the Seismological Society of America*, *110*(4), 1765–1780.

Ulrich, T., Vater, S., Madden, E. H., Behrens, J., van Dinther, Y., Van Zelst, I., Fielding, E. J., Liang, C., & Gabriel, A.-A. (2019). Coupled, physics-based modeling reveals earthquake displacements are critical to the 2018 Palu, Sulawesi tsunami. *Pure and Applied Geophysics*, *176*(10), 4069–4109.

Wald, D. J., & Heaton, T. H. (1994). Spatial and temporal distribution of slip for the 1992 Landers, California, earthquake. *Bulletin of the Seismological Society of America*, *84*(3), 668-691 %@ 1943-3573.

Wang, H., Liu, M., Duan, B., & Cao, J. (2020). Rupture propagation along stepovers of strike-slip faults: Effects of initial stress and fault geometry. *Bulletin of the Seismological Society of America*, *110*(3), 1011–1024.

Wang, H., Liu, M., Ye, J., Cao, J., & Jing, Y. (2017). Strain partitioning and stress perturbation around stepovers and bends of strike-slip faults: Numerical results. *Tectonophysics*, *721*, 211–226.

Wesnousky, S. G. (1988). Seismological and structural evolution of strike-slip faults. *Nature*, *335*(6188), 340–343.

Wesnousky, S. G. (2006). Predicting the endpoints of earthquake ruptures. *Nature*, *444*(7117), 358–360.

Wollherr, S., Gabriel, A.-A., & Mai, P. M. (2019). Landers 1992 “reloaded”: Integrative dynamic earthquake rupture modeling. *Journal of Geophysical Research: Solid Earth*, *124*(7), 6666–6702.

Ye, J., Liu, M., & Wang, H. (2015). A numerical study of strike-slip bend formation with application to the Salton Sea pull-apart basin. *Geophysical Research Letters*, *42*(5), 1368–1374.

Zhang, Z., Xu, J., & Chen, X. (2016). The supershear effect of topography on rupture dynamics. *Geophysical Research Letters*, *43*(4), 1457–1463.

Acknowledgement

This research is partly supported by SCEC grant 22144. Figures in this manuscript were generated using GMT (Wessel and Smith, 1998), Matplotlib (Hunter, 2007) and Paraview (available from https://www.paraview.com). I used the software Cubit version 21.5 to mesh the finite element models and FaultMod to compute the physics of the dynamic rupture simulations. I thank David Oglesby and Baoning Wu for fruitful discussion that helped moved this project forward.

List of Tables

P and S wave velocity	5480 m/s; 3160 m/s
Density	2700 kg/m^3
Radius of nucleation zone	5000 m
Hexahedral Mesh size	200 m
Slip-weakening distance (d_0)	0.4 m; 0.3 m
Static friction (μ_s)	0.75
Dynamic friction (μ_d)	0.30
Initial shear stress (τ_0)	10 MPa
Initial normal stress (σ_n)	16.65 MPa
S value ($\frac{\mu_s * \sigma_n - \tau_o}{\tau_o - \mu_d * \sigma_n}$)	0.5

Table 1: Model and frictional parameters for the dynamic rupture simulations

List of Figures

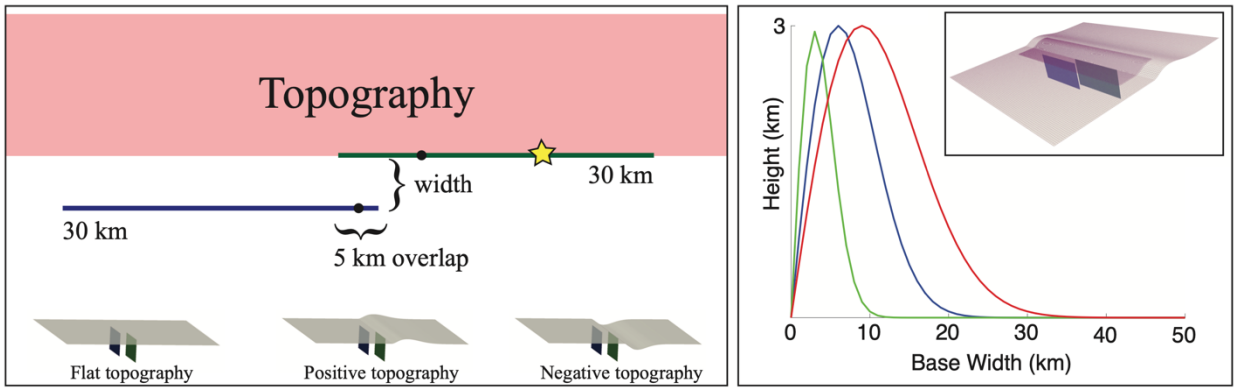

Figure 1: *The top part in the left panel shows the 2D sketch of the fault stepover configuration with the topography in map view. Fault 1 or ruptured fault is shown in green and fault 2 in blue. The red shaded area marks the position of topography (positive or negative). The yellow star shows the location of the nucleated point. The black dots mark the locations where I evaluate slip, shear and normal stresses time histories (see figure 5). The bottom part of the left panel shows the 3D views for the flat, positive, and negative topography cases. The right panel shows the 2D Rayleigh distribution of topography with respect to fault 1 located at the origin. The red, blue, and green distributions are for a base width of 30, 20 and 10 km respectively (see Figure 8). The inset in the right panel shows the finite element mesh.*

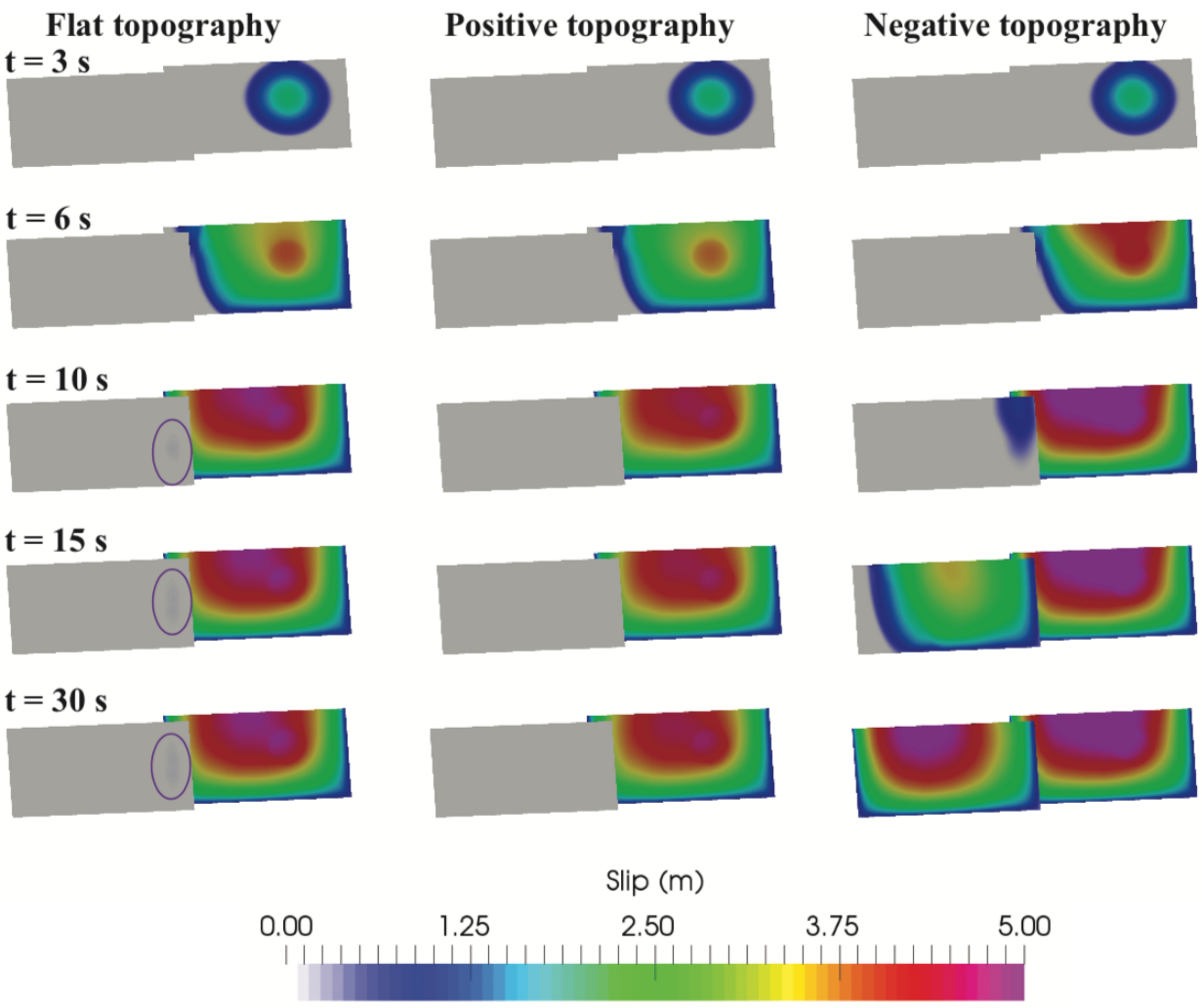

Figure 2: *Snapshots of the slip distribution at different time steps for the flat, positive and negative topography cases for a slip weakening distance of 0.4 m. The bottom row is the final slip distribution. The purple ellipse on the flat topography case marks the location where rupture triggers on the receiver fault but rapidly dies out.*

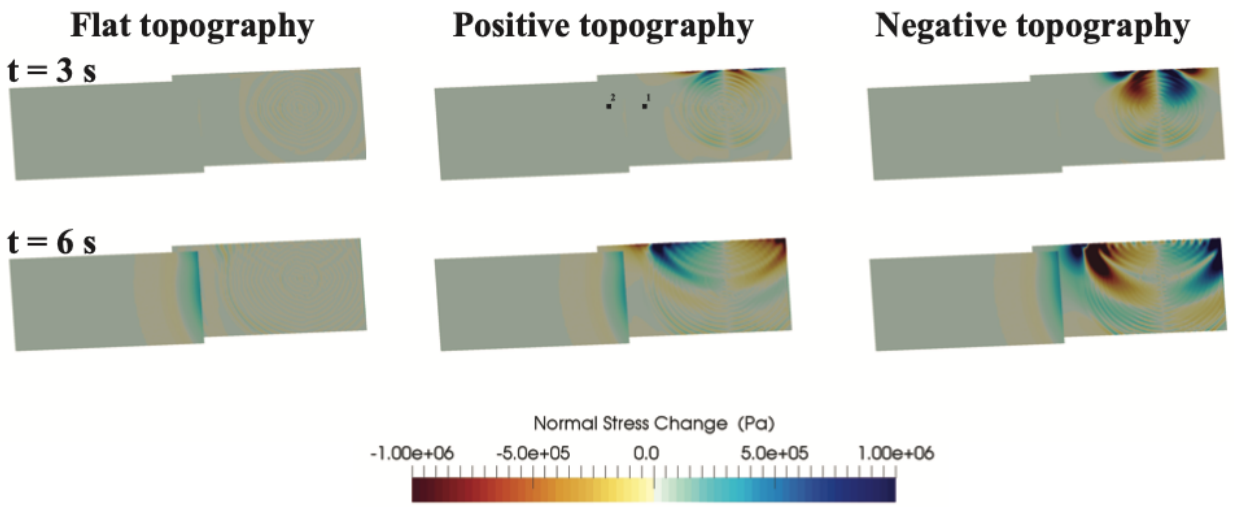

Figure 3: *Snapshots of the normal stress change at time steps 3 and 6 s for the flat, positive and negative topography cases. Blue color indicates a clamping effect and red an unclamping effect. The black dots 1 and 2 on fault 1 and fault 2 respectively mark locations where I evaluate slip, shear stress and normal stress time histories (see Figure 4). For this extensional stepover, a positive topography causes an increase of the normal stress behind the rupture front while a negative topography causes a decrease of the normal stress behind the rupture front.*

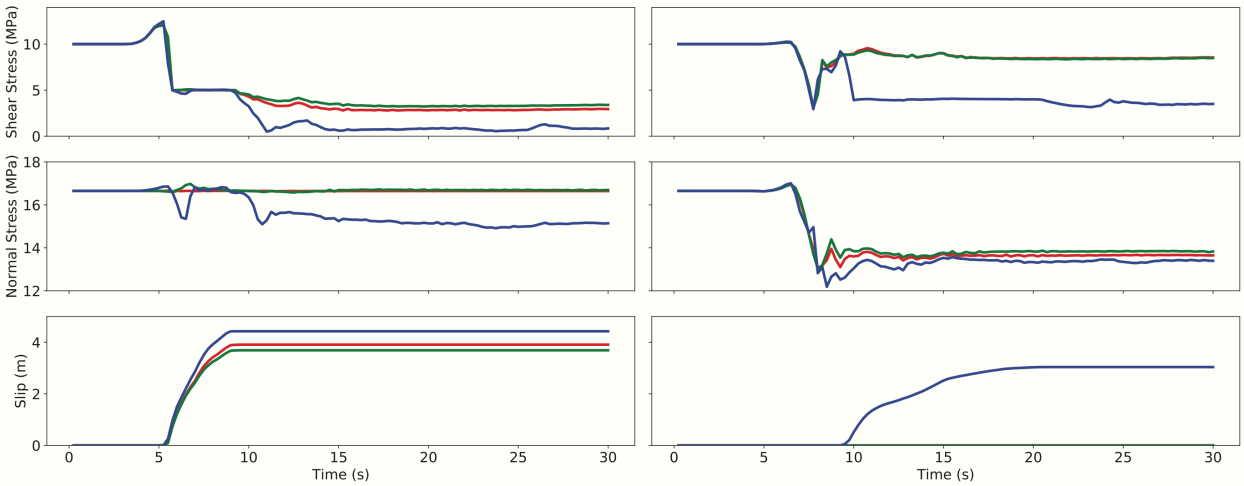

Figure 4: *Slip, normal stress and shear stress histories for point 1 on fault 1 (1st column) and point 2 on fault 2 (2nd column). The locations of those two points are shown in Figure 1. Red, green and blue lines show the result of the flat, positive and negative topography cases respectively for a slip-weakening distance of 0.4 m and a stepover width of 4 km.*

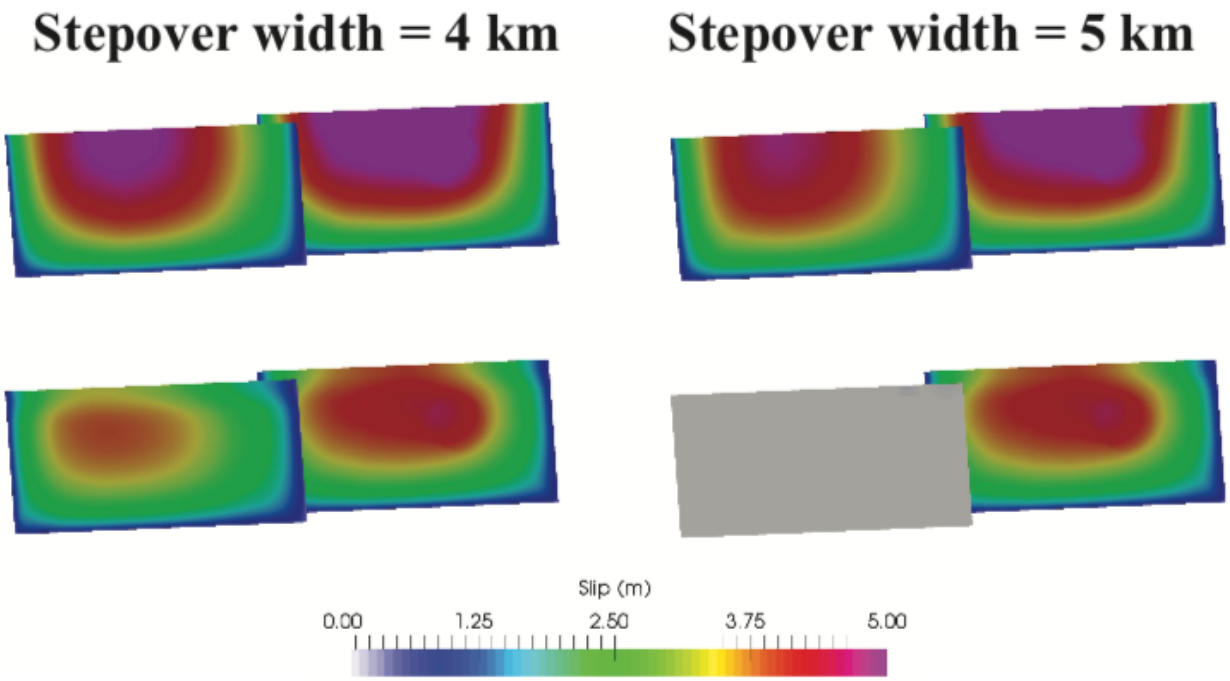

Figure 5: *Final slip distribution for the negative topography, for an extensional stepover width of 4 km (1st column) and 5 km (2nd column) and for a slip-weakening distance of 0.4 m. The upper row shows results for homogeneous stress conditions and the bottom row shows results where the shear and normal stresses are tapered linearly.*

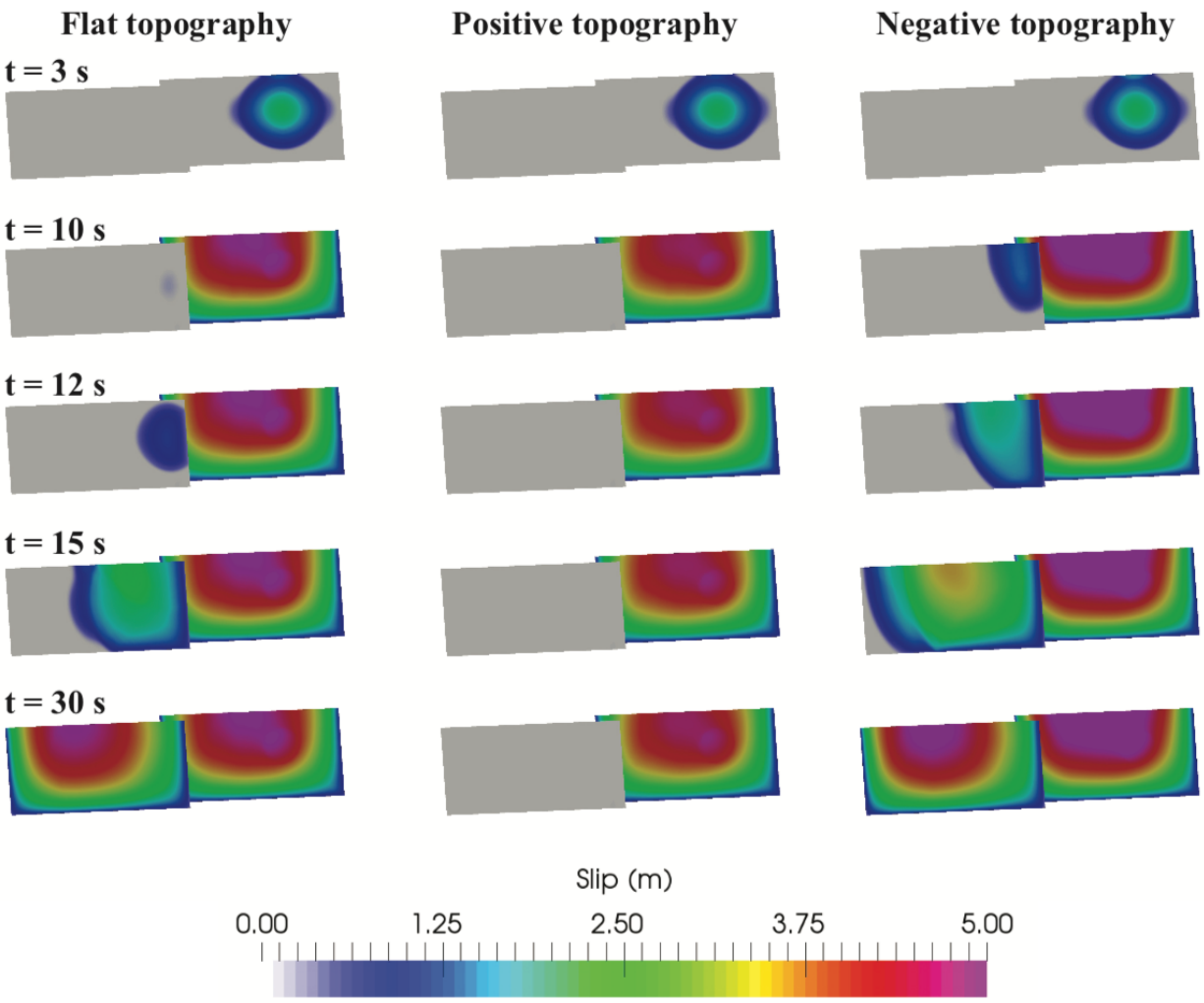

Figure 6: *Snapshots of the slip distribution at different time steps for the flat, positive and negative topography cases for a slip weakening distance of 0.3 m and stepover width of 4 km. The last line is the final slip distribution.*

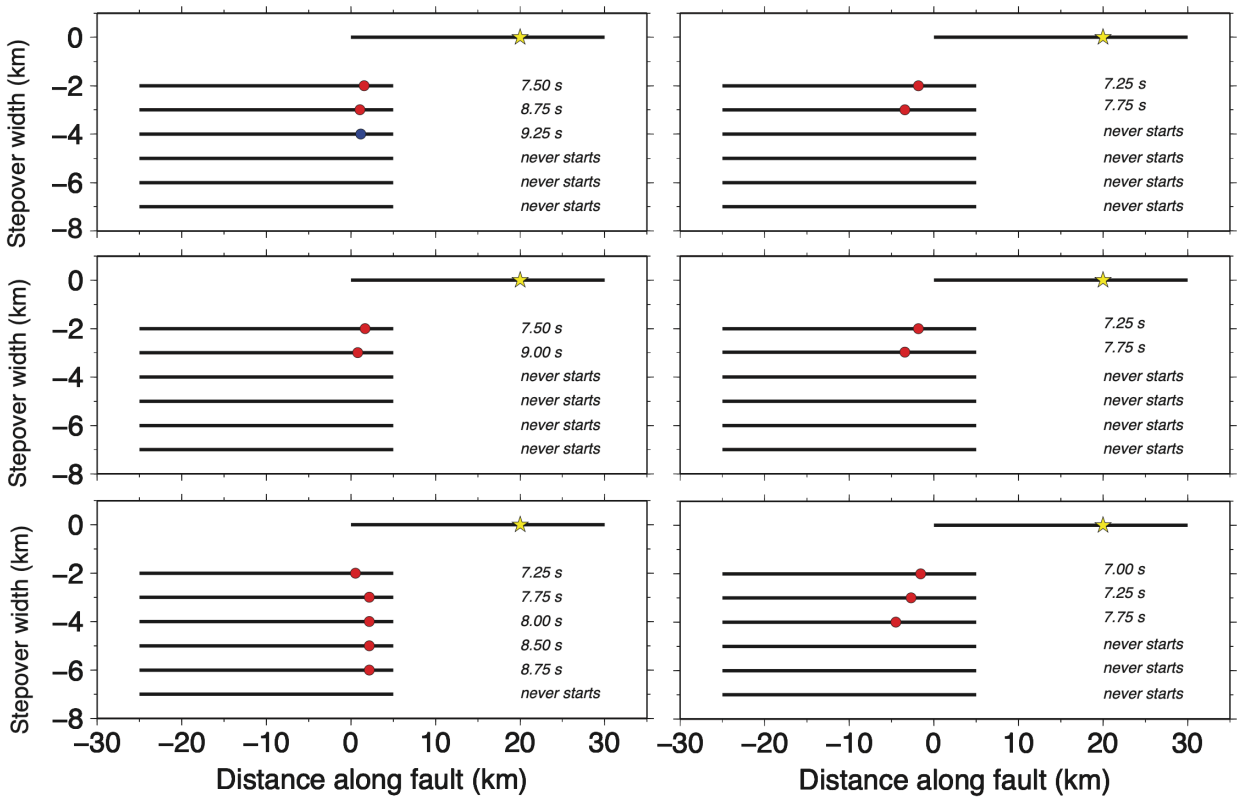

Figure 7: *Summary of rupture behavior for various stepover widths for the 0.4 m slip weakening case. The left column shows the extensional stepover (left-lateral strike-slip) and the right column the compressional stepover (right-lateral strike-slip. The top, middle and bottom panels are for a flat, positive and negative topography respectively. The yellow star marks the location of the nucleation point on fault 1. The circles show the locations of the initial triggering point on fault 2 and the time when rupture on fault 2 is triggered are shown on the right for each case. A red circle indicates that fault 2 breaks entirely while a blue circle indicates that rupture dies out on fault 2.*

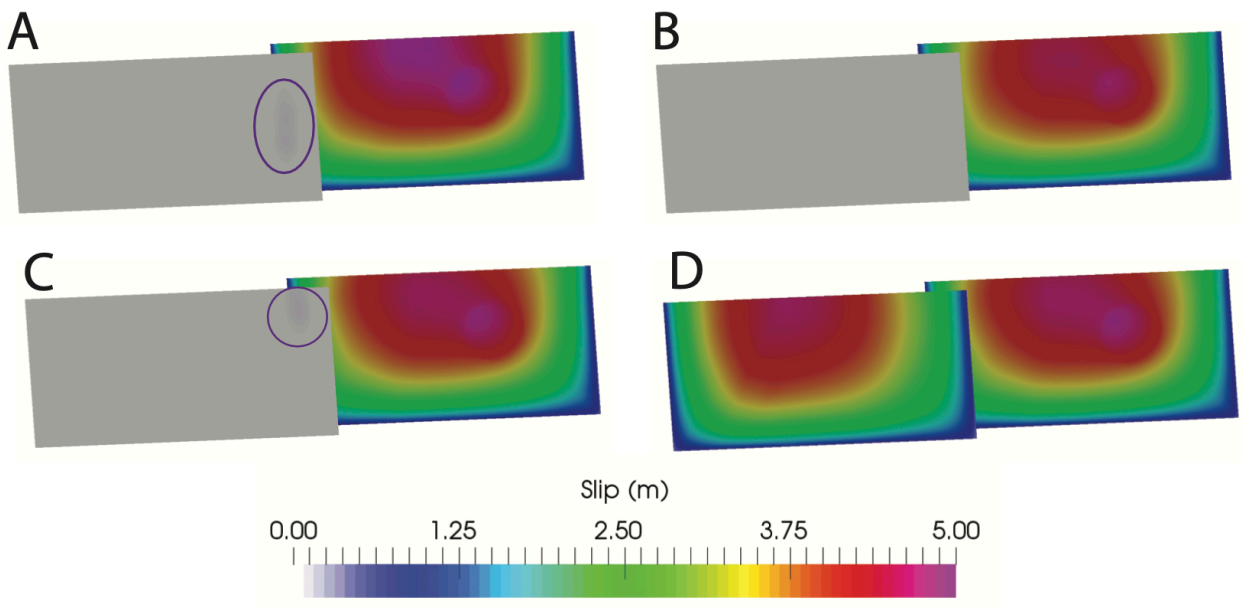

Figure 8: *Final slip on an extensional stepover width of 4 km with a slip-weakening distance of 0.4 m. Panel A marks the flat topography case, same as in Figure 2; panel B is for positive topography width of 30 km, same as in Figure 2; panel C is for a positive topography width of 20 km and panel D is for a positive topography width of 10 km.*

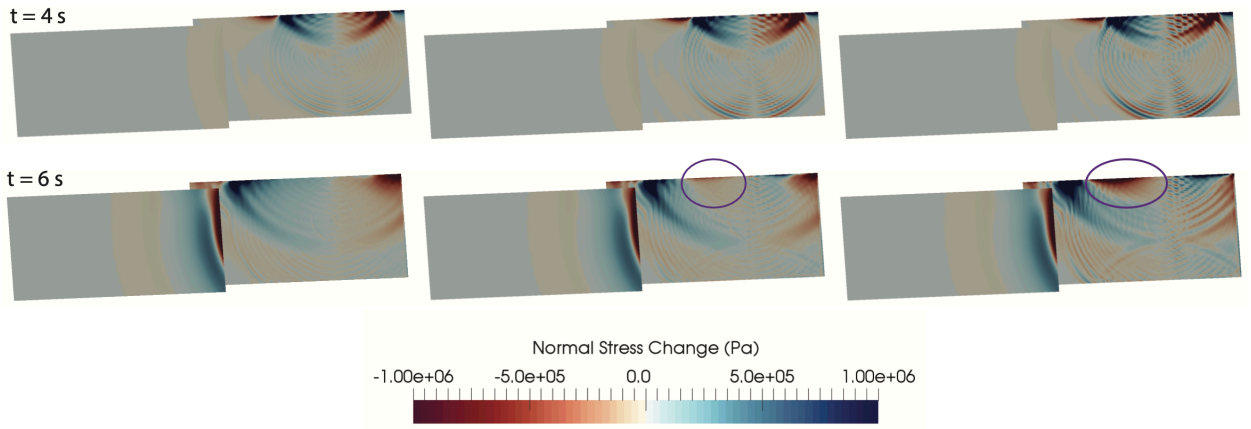

Figure 9: *Snapshots of the normal stress change at time steps 4 and 6 s for the positive topography width of 30 km (1st column, same as in Figure 4), 20 km (2nd column) and 10 km (3rd column). For this extensional stepover, positive topography causes an increase of the normal stress behind the rupture front followed by a decrease only for the narrower topography (20 and 10 km) as shown by the purple ellipse. This subsequent decrease of the normal stress can lead the rupture to jump across the extensional stepover.*

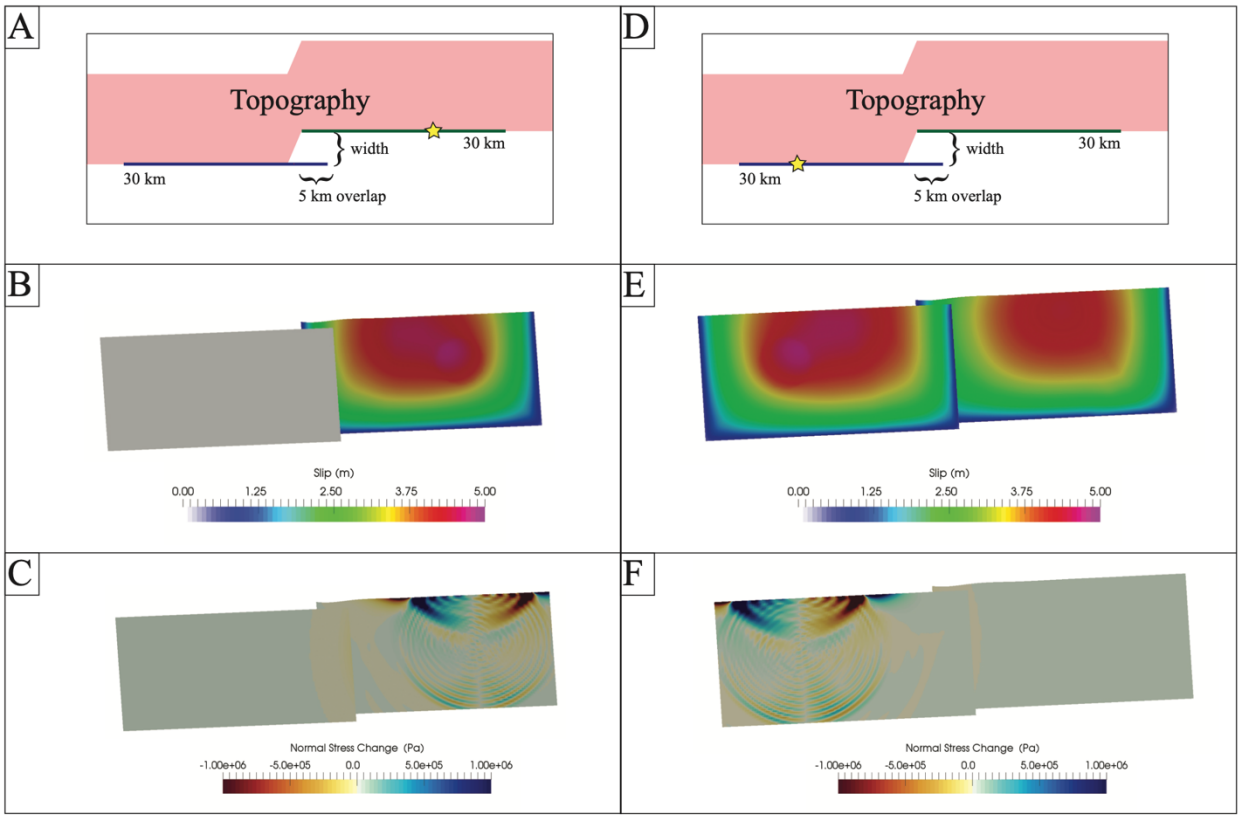

Figure 10: Left column shows the sketch and dynamic simulation for a rupture initiated on fault 1 and the right column is for a rupture initiated on fault 2. Panels A and D show the new 2D sketch of the fault stepover configuration with the position of the positive topography (red shaded area) in map view. The yellow star shows the location of the nucleated point. Panels B and E show the final slip on an extensional stepover width of 4 km with a slip-weakening distance of 0.4 m and panels C and F mark the snapshot of the normal stress change at 4 s. For the rupture initiated on fault 2, the decrease in normal stress behind the rupture front allows the rupture to propagate on fault 1.